Title

ELECTRON MICROSCOPY STUDIES OF DEFECTS IN BORON-SINTERED CUBIC SILICON CARBIDE

Author

Dizon, Fernando De Los Santos.

Publication Date

1977-05-01

Thesis/dissertation

UC-25
LBL-6269
c.1

ELECTRON MICROSCOPY STUDIES OF DEFECTS IN BORON-SINTERED CUBIC SILICON CARBIDE

Fernando de los Santos Dizon
M.S. thesis

May 1977

This work was done with support from the U. S. Energy Research and Development Administration

LBL-6269
c.1

DISCLAIMER

LBL-6269

ELECTRON MICROSCOPY STUDIES OF DEFECTS IN BORON-SINTERED CUBIC SILICON CARBIDE

Fernando de los Santos Dizon
M. S. thesis

May 1977

This work was done with support from the U. S. Energy Research and Development Administration

LBL-6269

CONTENTS

ELECTRON MICROSCOPY STUDIES OF DEFECTS IN BORON-SINTERED CUBIC SILICON CARBIDE

Fernando de los Santos Dizon

Abstract

Intra-granular defects in boron-sintered cubic silicon carbide have been studied using transmission electron microscopy. Planar faults and dislocations were examined. Closely spaced faults permeating a majority of grains were observed and analyzed, but the Burgers vectors of the terminating partial dislocations could not be uniquely determined since the faults extended to the grain boundaries. Thus, the faults could not be distinguished as growth or shear type. Isolated faults were also observed and characterized as extrinsic. Dislocation dipoles and networks of other dislocations were observed. These were likely to have been formed by deformation at the high sintering temperatures. A possibility remains that the networks observed were present in the crystallites prior to sintering.

Section I

INTRODUCTION

Some desirable performance objectives for gas turbines used for power production include improved efficiency, lower initial cost, and extended engine life. These objectives are, at present, limited by the properties of super-alloys used in these turbines. These materials can be operated only at surface temperatures of less than about 900°C unless cooling is used. The engine life of gas turbines is limited mainly by the poor corrosion-erosion resistance of these alloys when used at high temperatures. The susceptibility of super-alloys to impurities found in dirty residual fuels limits their fuel economy. The necessity for cooling increases the initial blade costs and decreases their power output.[1]

Ceramics such as silicon nitride and silicon carbide may overcome many of the limitations that the use of super-alloys imposes on the improved performance of gas turbines. Since ceramics have refractory properties, they can be used at surface temperatures exceeding 900°C without cooling. This is an important asset since the engine efficiency increases with higher operating temperatures. Ceramics have superior corrosion-erosion resistance and are able to tolerate the contaminants found in residual fuels.

Unfortunately, ceramic parts cannot be substituted directly for parts which now use super-alloys. The inherent brittleness of ceramics places doubt on their mechanical performance in these turbines. Addi-

tionally, more efficient and reproducible fabrication techniques need to be perfected for ceramics so that fabrication costs decrease and the results from testing can be correlated to known microstructures.

For silicon carbide, one step towards its intended use in turbines has been made. The General Electric Co. has invented a process which employs boron in the sintering of the cubic form of silicon carbide. The addition of boron makes possible pressureless sintering with concurrent high densities. The reproducibility of this fabrication technique is satisfactory.[2]

Once the material can be reliably produced with a uniform microstructure, it has to be tested under the conditions anticipated for high temperature gas turbines. Descriptions of thermal and mechanical testing can be found in reference (1). What is also needed, though, is a correlation between the microstructure and the results from these thermal and mechanical tests.

The initial steps in determining the microscopic defect structure of the sintered cubic form of silicon carbide are described in this thesis. Transmission electron microscopy was chosen for its capability of resolving the microscopic intra-granular defects in this fine-grained form of the material. Combined with diffraction information, the character of the defects was determined. Both planar faults and dislocations were investigated. Very closely spaced faults which permeated the majority of grains in the material were studied because they formed the major defect structure observed. Isolated stacking faults were also investigated and characterized as extrinsic faults. Dislocations in the form of dipole pairs made up the majority of the low total dislocation density found in this ceramic material.

Other dislocations, in addition to the dipoles were observed. Grains, in which these dislocations were found, exhibited electron diffraction patterns which suggested the existence of a superlattice in the crystallographic structure of cubic silicon carbide.

The structure and crystallography of silicon carbide will be discussed as well as the body of previous work pertaining to the characterization of defects in this material. After a description of the experimental procedure, each defect examined will be described and discussed.

Section II

STRUCTURE AND CRYSTALLOGRAPHY OF SILICON CARBIDE

A. General Structure

While the particular form of silicon carbide studied was the cubic form designated as β, it is worthwhile to discuss this structure in a broader context encompassing other forms of SiC.

Silicon and carbon are both quadrivalent elements. This fact has two consequences. The first is that both the carbon and the silicon atoms are tetrahedrally coordinated, namely with four nearest neighbors of the opposite atomic species. The second consequence is that the nearest neighbor bonds are covalent. Thus, the appropriate coordinating polyhedron which determines the short range structure is a tetrahedron consisting of silicon at the center with carbon at the corners (or vice-versa). Thus all silicon carbide structures are made up of a single basic unit consisting of a plane of these tetrahedra, shown in Fig. 1. The long range differences in the structures are determined by two factors: (1) the orientation of successive layers of tetrahedra with respect to each other, and (2) the stacking sequence of these layers.

There are several systems of nomenclature used for describing the various SiC structures. These systems, in one way or another, describe both of the factors mentioned in the preceeding paragraph. The notation ascribed to Wells[3] gives each plane of tetrahedra one of two names, either 'a' or 'b'. If the first layer of tetrahedra is

designated as 'a', the second layer may be placed on it in one of two possible ways--either parallel (Fig. 2a) or anti-parallel (Fig. 2b). A parallel stacking sequence results in the designation 'aa', and anti-parallel as 'ab'. In Well's notation, the smallest repeating unit of the particular silicon carbide structure being described is used to designate the structure. Thus, the cubic modification is designated simply as 'a', since all succeeding tetrahedral layers are stacked in the parallel manner. Examples of other known structures are aabb, aaabbb, and aaabb.

The notation due to Zhdanov and Minervina[4] and Mitchell[5] is a compression of the Wells notation, e.g., aabb becomes '22', namely, two layers stacked parallel, and the next two stacked similarly with respect to each other, but differing from the first pair.

Ramsdell's notation[6] represents a specific SiC structure by the number of layers in the unit cell together with a letter designating the lattice type, e.g., 6H, 15R, and 3C are Ramsdell notations for structures with respectively 6, 15, and 3 layers in the unit cell and with hexagonal, rhombohedral and cubic lattices. In Well's notation these are respectively aaabbb, aaabb, and 'a'.

These notations are the ones in common usage in the literature. Other systems of nomenclature are given by Verma and Krishna[7] and are attributed to several other workers.

Shaffer[8] and deMesquita[9] have reviewed the details of the crystal structure of the known polytypes of SiC. Specifically, for this thesis, the cubic form, i.e., β-SiC or 3C (Ramsdell's notation) has been investigated. The atomic positions of the silicon and carbon atoms in this

structure are:

Silicon: $0\ 0\ 0 \quad 0\ \frac{1}{2}\ \frac{1}{2} \quad \frac{1}{2}\ 0\ \frac{1}{2} \quad \frac{1}{2}\ \frac{1}{2}\ 0$

Carbon: $\frac{1}{4}\ \frac{1}{4}\ \frac{1}{4} \quad \frac{1}{4}\ \frac{3}{4}\ \frac{3}{4} \quad \frac{3}{4}\ \frac{1}{4}\ \frac{3}{4} \quad \frac{3}{4}\ \frac{3}{4}\ \frac{1}{4}$

The lattice parameter is 4.348Å. The C-Si bond, of length 1.89Å, is the shortest inter-atomic distance. The C-C and Si-Si bonds are of length 3.09Å in this structure.[10]

B. Crystallography of Defects

The overall crystal structure of β-SiC (the cubic form) has been described in terms of the infinite "parallel" stacking of tetrahedral layers (viz. aaa... in Well's notation) and the designation of atoms positions in the unit cell. Neither of these descriptions lend themselves easily to the description of planar and linear defects in the structure.

For the description of these defects it is first of all, necessary to know what the perfect dislocation Burgers vectors are in the structure. The dislocations can then be described and the splitting of these dislocations into partial dislocations leads to the description of the planar faults. The structure of β-SiC can be visualized as corresponding to two inter-penetrating fcc lattices, one of which is displaced by the vector $\frac{1}{4}$ [111] with respect to the other (Fig. 3). One fcc lattice consists entirely of silicon atoms and the other of carbon atoms. The structure can then be described as an fcc structure with a basis of two atoms per lattice point. The primitive unit cell vectors are those associated with the single fcc lattice

i.e., a/2 ⟨110⟩. These are also the shortest lattice translation vectors and thus, are candidates for the Burgers vectors of dislocation in the structure.

1. Planar Faults

In regular fcc structures, the stacking of {111} planes follows the classic ABCABC ... sequence. But in β-SiC there are two interpenetrating fcc structures which means that the layer structure can be described as planes in the double letter sequence: AaBbCcAa BbCc.

In Fig. 4, the β-SiC lattice is projected normal to $(1\bar{1}0)$. In this projection the (111) layers A and a are seen to project to the same type of position, as do B and b and also C and c. Looking at this particular projection, a more suggestive notation is given by the sequence cA aB bC cA, because of the larger separation between atoms in the same index layer, i.e. A and a. Twins and stacking faults involve the insertion or removal of pairs of layers of the same index, Aa, etc.

Since layers are removed or added in pairs, it is possible to drop the double index notation and describe the packing by the sequence ABCABC ... (as in a regular fcc structure) but in this case each letter refers to a pair of layers.

The requirement that layers must be removed or added in pairs makes the description of stacking faults in β-SiC a matter of analogy with basic fcc structures. The intrinsic fault in fcc structures is obtained by the removal of a plane of atoms. In β-SiC this involves

the removal of a double layer of atoms. This is shown in Fig. 5a and the fault is designated ABC¦BCAB. Similarly, the extrinsic fault is obtained by the addition of a double layer and is denoted by CA¦C¦BC. This fault is shown in Fig. 5b.[11]

2. Dislocations

The covalent nature of the bonds in SiC makes it possible to attempt a description of the atomic arrangements in the cores of the dislocations since these bonds can be regarded as directed in space. Hornstra[12] describes the dislocations in diamond and Holt[13] used the same methods for the dislocations in the sphalerite structure of which β-SiC is an example. The work of these two authors gives a starting point for discussing the geometrically possible dislocation structures in β-SiC.

In Fig. 4, the $(1\bar{1}0)$ was shown in discussing the planar faults. This same projection, shown clinographically in Fig. 6a, serves to describe the geometrically feasible dislocations in β-SiC.

The combinations of stable Burgers vectors $\underset{\sim}{b}$ and low index crystallographic line directions $\underset{\sim}{a}$ give all the simple dislocations which differ in core structure. The two directions $\underset{\sim}{b}$ and $\underset{\sim}{a}$ determine the slip plane of the dislocation (for screw dislocations, $\underset{\sim}{b}$ and $\underset{\sim}{a}$ are parallel and a plane may be arbitrarily chosen).[13]

The steps in determining the core structure of a dislocation in the β-Sic structure is shown in Fig. 6. The 60° dislocation (so called because of the angle between $\underset{\sim}{a}$ and $\underset{\sim}{b}$) can be "constructed" by first considering the (111) slip planes and their respective puckered

sheets of silicon and carbon atoms. Choosing $b = a/2[\bar{1}01]$ and $a = [1\bar{1}0]$ on this plane, these vectors are represented in Fig. 6a. In 6b the result of moving this 60° dislocation into the crystal from right to left is to produce the relative movements of the atoms indicates by the arrows. Then the atoms above the slip plane are displaced to the right through $a/2[\bar{1}01]$ relative to those below. The proposed core structure, then, is visualized by connecting up nearest neighbors across the slip plane in a way consistent with the simplest picture of a covalent bond. This is shown in Fig. 6c.

Holt[13], in discussing defects in the sphalerite structure, has drawings showing schematic representations of other possible dislocations in this structure. Table 1 lists the geometrically feasible dislocations in sphalerite type structures.

Table 1

Dislocations in Sphalerite Structures

Description	$\underset{\sim}{b}$	$\underset{\sim}{a}$	Glide Plane
Screw	$\frac{a}{2}\langle 110\rangle$	$\langle 110\rangle$	Not defined
60°	$\frac{a}{2}\langle 110\rangle$	$\langle 110\rangle$	{111}
Edge	$\frac{a}{2}\langle 110\rangle$	$\langle 110\rangle$	{100}
Small Angle Boundary Dislocation	$\frac{a}{2}\langle 110\rangle$	$\langle 001\rangle$	{110}
--	$\frac{a}{2}\langle 110\rangle$	$\langle 110\rangle$	{001}
Edge	$\frac{a}{2}\langle 110\rangle$	$\langle 112\rangle$	{111}
30°	$\frac{a}{2}\langle 110\rangle$	$\langle 112\rangle$	{111}

The double layer structure of sphalerite structures introduces an additional complexity in the description of possible core structures. The 60° dislocation described in Fig. 6, is now seen along its line direction in Fig. 7. The carbon atoms are represented by the black dots and the silicon atoms by the circled black dots. In this figure the double layer atomic arrangements is apparent as is the possibility of two types of {111} slip planes, type I and II. The 60° dislocation is shown with its extra half plane ending at a type II plane, where it breaks the least number of bonds. The one bond per atom which is broken has been described as a dangling bond. The dislocation, as pictured, is a member of the shuffle set of dislocations as defined by Hirthe and Lothe[11] and is the same 60° dislocation described by Holt.[13] Had the dislocation passed through the type I plane, the 60° dislocation would have been pictured as in Fig. 8. The distinction between Type I and Type II glide planes holds for screw and edge dislocations as well as intermediate orientations. The 60° dislocations have been described in detail not only because of their ease of depiction but also because they were the type observed in this research.

Section III

PREVIOUS WORK ON SILICON CARBIDE

There have been very few theoretical or experimental studies of dislocations in SiC. The studies that have been made mainly on fracture chips. R. Stevens[14] studied fracture chips of self-bonded β-SiC. He identified dislocations with Burgers vector $\underset{\sim}{b} = \frac{a}{2}\langle 110\rangle$ and the operating slip plane as {111}. Stevens noted that the generation of motion for the dislocations he observed could occur only on a limited scale and are probably due to the special conditions of stress concentrations occurring at the crack front of the fracture chip. In other words, the dislocations he observed were not representative of the dislocation structure before fracture.

Additional electron microscopy was performed, again by Stevens,[15] on specimens of β-SiC fractured at 1100°C. Tangles of dislocations containing dipoles and jogs were observed. No analysis supporting the characterization of these dislocations as dipoles and jogs was presented.

Stevens[16] extended his study of silicon carbide into an investigation of the hot-pressed forms. Both β-SiC and α-SiC (hexagonal) were investigated. The most striking feature in the foils examined by TEM was the scarcity of dislocations. Stevens, in this paper, does not present a detailed characterization of the dislocations he observes. Neither does he report any attempts to ascertain the displacement vector of the stacking faults in the material.

Bartlett and Martin,[17] although not performing transmission electron microscopy on SiC, were able to study general features of the defect structure of β-SiC using Lang X-ray topography, Weissenberg photographs and etch pit analysis. The only defects seen were stacking faults on {111} planes with associated $\frac{1}{6}\langle 112\rangle$ partials and a few {111} twins on planes parallel to the growth plane of the platelets.

L.I. Van Torne[18] examined silicon carbide whiskers grown from the vapor using transmission microscopy. Nearly 95% of the whiskers examined were of the β form and contained stacking faults on {111}. The stacking faults formed micro twins of the order of a few lattice parameters (12.5Å). Cromer[19] also did work on β-SiC grown from the vapor and supported some of Van Torne's predictions. He found evidence, using dark field microscopy and selected area diffraction, for multiple twinning along the [111] axis of the whisker, with the twins being related to each other by a rotation of 180° about the growth axis. Stevens,[16] observing the same type of twins that Van Torne and Cromer found, also found evidence for the twin plane occurring parallel to the axis of the whisker.

Stacking faults in chemically-vapor-deposited (CVD) β-SiC were investigated by Gulden.[20] The results of this investigation showed that growth faults in CVD β-SiC are most likely to be in the form of simple extrinsic faults with displacement vector $\frac{1}{3}\langle 111\rangle$. Gulden presents an intensive investigation of the faults, outlining the electron diffraction contrast analysis leading to the identification of the displacement vector and the nature of the faults. The fringe

patterns presented by the faults showed conclusively that stacking faults and not anti-phase boundaries, twin boundaries, or plate shaped precipitates were responsible for the contrast.

Much of the further work was done on the hexagonal forms of SiC. Van Landuyt and Amelinckx[21] studied the 6H polytype. They found a few stacking faults in the basal plane, each having a displacement vector $\frac{1}{6}\langle 2\bar{2}01\rangle$ with some connected segments in the prismatic planes. Work by Drum[22] showed basal plane stacking faults in α-silicon carbide single crystals.

For completeness, it is worthwhile to mention that in addition to the work on dislocations and stacking faults, another important area of investigation in SiC is its polytypism. A recent work on polytypism in SiC is by Yessik, Shinozaki, and Sato.[23] In this study transmission electron microscopy was used to determine the structures of four long-period poly types of SiC found in a sample of reaction sintered material. It should be mentioned that among these polytypes none were of the cubic form.

Worthington[24] reports on the observation of polytypes and stacking faults in zinc sulphide by transmission microscopy. While this was not specifically done on β-SiC, it is appropriate to mention it here for several reasons. First, cubic zinc sulphide is isostructural with β-SiC. In fact, Worthington's paper shows micrographs and diffraction patterns which are similar to those observed in the β-SiC investigated for this thesis. Specifically, diffraction patterns from the ⟨110⟩ type orientations show streaking and extra spots which will be presented later on in this thesis. And more striking, the striation-

filled grains from the ZnS are reminiscent of grains in β-SiC. Worthington states that these striations may be attributed to faults in the basal plane stacking sequence. He makes the observation that the striations could no longer be seen when the specimen was oriented so that the reciprocal lattice vector, $\underset{\sim}{g}$, of the operative reflection was perpendicular to the striations, implying that the displacement vector of the stacking fault responsible for the appearance of the striation lies in the basal plane.

Section IV

EXPERIMENTAL PROCEDURE

Specimens of β-SiC suitable for transmission electron microscopy were prepared in the following manner. Wafers, approximately 500 μm thick were sectioned from the bulk material with a diamond wafering blade. 2.3 mm DIA. discs were ultrasonically cut from these wafers and then mounted onto glass slides for mechanical thinning. After thinning to ~60 μm the discs were mounted with epoxy, on 3 mm DIA. specimen grids for the final step in the specimen preparation process--ion milling. Using a beam current of ~10 μA and an accelerating voltage of 5 kV, the discs were bombarded with argon ions until small holes in the center were visible.

The edges of these holes, were thin enough to allow penetration of the electron beam accelerated through a potential of 100 kV in the Philips EM 301 electron microscope. Additional microscopy was performed with the Hitachi HU-650 high voltage microscope operating at 650 kV.

The goniometer stage for the EM301 as well as the double-tilt stage for the HU-650 were used to obtain the two beam or systematic row conditions necessary for analyzing crystal defects such as dislocations and stacking faults.

SECTION V

RESULTS AND DISCUSSION

A. Planar Faults

1. Closely Spaced Faults

Results

A scanning electron micrograph of the etched surface of boron-sintered β-SiC reveals the small grain size of the material. From this micrograph the grain size was estimated to be on the order of 10 μm (Fig. 9). (Etching was accomplished by immersion of the specimen, for 30 seconds, in a 50:50 mixture of sodium nitrite and sodium peroxide brought to 500°C).

The transmission microscope revealed that the majority of these grains were heavily faulted. Figure 10 shows an example of such a grain. The diffraction condition was two-beam with the operating reflection being $20\bar{2}$ near the [101] symmetric orientation. The planar faults are seen edge-on (circled area in Fig. 11a) when the grain is tilted to this symmetric orientation. Only the $(11\bar{1})$ planes are seen to be faulted. The faulting on $(11\bar{1})$ is evidenced by streaking through each of the reciprocal lattice points in the [101] orientation (Fig. 11b). Additionally the extra spots along $[\bar{1}\bar{1}1]$, through all the reciprocal lattice rows, shows evidence for periodic faulting.

The heavy faulting, observed in this grain, became invisible when two-beam diffraction conditions were obtained for the reflections $2\,\bar{4}\,\bar{2}$, $2\bar{2}0$, and $11\bar{1}$ (Fig. 12).

Discussion

The investigation of the faulting in the heavily striated grains led to the determination of a displacement vector for these faults. This vector $\underset{\sim}{R}$, for planar defects represents the magnitude and direction by which the atoms on one side of the fault have been moved with respect to their positions in the perfect crystal.

In the theory for explaining the contrast due to planar faults, the value of the phase angle $\alpha = 2\pi \underset{\sim}{g} \cdot \underset{\sim}{R}$ (where $\underset{\sim}{g}$ is the operating reflection) is an important parameter which determines the visibility of the faults. When α is equal to zero or to an integral multiple of 2π, the fault becomes invisible.[25]

For the striations, the vector $\underset{\sim}{R} = \frac{1}{3}[11\bar{1}]$ is a vector which gives the values, 0, 2π, and 0 when evaluating α, respectively, for the reflections $2\bar{2}0$, $11\bar{1}$, and $2\,\bar{4}\,\bar{2}$. These reflections were those for which the striations were invisible. But the displacement vector $\underset{\sim}{R} = \frac{1}{3}[11\bar{1}]$ is not the only vector for which $\alpha = 0, 2n\pi$. The addition of a lattice translation vector $\underset{\sim}{t} = \frac{a}{2}\langle 110\rangle$ to $\underset{\sim}{R}$ will still give $\alpha = 0, 2n\pi$ since $2\pi \underset{\sim}{g} \cdot \underset{\sim}{t} = 2n\pi$ for any $\underset{\sim}{t}$.

Ultimately, this uncertainty in ascertaining $\underset{\sim}{R}$ can be resolved by determining the Burgers vector $\underset{\sim}{b}$ for partial dislocations at the boundary of these faults. Unfortunately, the faults in these heavily striated grains all terminated at the grain boundary, which made it impossible to resolve any partial dislocations. Thus, the question of whether the faults are due to growth or shear is still unanswered. Specifically, not only does the displacement vector $\underset{\sim}{R} = \frac{1}{3}[11\bar{1}]$ satisfy the invisibility conditions, but also the three $1/6\langle 112\rangle$ vectors in

the $(11\bar{1})$ plane. Explicitly:

$$\frac{1}{3}[11\bar{1}] + \frac{1}{2}[1\bar{1}0] = \frac{1}{6}[\bar{1}\bar{1}2]$$

$$\frac{1}{3}[11\bar{1}] + \frac{1}{2}[0\bar{1}1] = \frac{1}{6}[2\bar{1}\bar{1}]$$

$$\frac{1}{3}[11\bar{1}] + \frac{1}{2}[\bar{1}01] = \frac{1}{6}[\bar{1}21]$$

Thus, up to an uncertainty in a lattice vector, $\underset{\sim}{R}$ can be defined, for the heavy faulting as $1/3\langle 111\rangle$ or $1/6\langle 112\rangle$.

As noted in Section III, Worthington[24] attributes the displacement vector to one found in the basal plane (i.e., the plane of faulting) in cubic ZnS which is isostructural with β-SiC. It cannot be stated that these faults have specifically, a displacement vector in the fault plane since, again, the addition of a lattice vector to $\underset{\sim}{R}$ would transform it to a displacement vector perpendicular to the fault plane and still not affect the contrast.

While the microscopy performed, concentrated on the characterization of the displacement vector of the faults, there remained the problem of explaining the complex diffraction pattern of the $\langle 110\rangle$ symmetric orientation in which these faults were seen edge-on (Fig. 11a). Headway into solving this problem has been made by D. R. Clarke using the lattice imaging technique.[25] The existence of various SiC polytypes other than β-SiC is revealed directly by this technique and also serves as a correlation with the periodic faulting indirectly evidenced by the selected area diffraction pattern.

2. Extrinsic Faults

Results

While heavy faulting was observed in the majority of grains there were instances where grains were observed with a lesser degree of faulting. An example is shown in the micrograph of Fig. 13. As with the striations, the contrast is determined by the phase angle $\alpha = 2\pi \underset{\sim}{g} \cdot \underset{\sim}{R}$ with invisibility occurring for $\alpha = 2n\pi$, $n = 0,1,2,3$. The fault marked F shows fringe contrast which can be ascribed to stacking faults characterized by a phase angle, α, equal to $+ 2\pi/3$. The fault disappeared for the reflections $\bar{1}\,\bar{1}\,3$, $1\,\bar{1}\,\bar{1}$, and $02\bar{2}$ (Fig. 14). The disappearances are consistent with a displacement vector, $\pm \frac{1}{3}[1\,\bar{1}\,\bar{1}]$.

Discussion

The nature of the fault, whether intrinsic or extrinsic, was determined from a detailed analysis of the fringe contrast. For stacking faults in fcc materials, the sign of the phase angle α is determined solely by the color of the edge fringes in the bright field condition.

Figure 15 shows a BF-DF pair of the same area under the operating reflection $g = \bar{2}02$. The color of the edge fringes, in BF, is dark indicating that $\alpha = -2\pi/3$. The displacement vector $\underset{\sim}{R} = \frac{1}{3}[1\,\bar{1}\,\bar{1}]$ is consistent, under $g = \bar{2}02$, with a phase angle $\alpha = -2\pi/3$. The inclination of the fault plane is determined from the contrast of the edge fringes in both BF and DF. According to Hirsch et. al.[26], the edge fringes are pseudo-complementary at the intersection of the bottom of the fault with the surface. This, as must be pointed out, is true for a low-resolution DF, i.e. where the objective aperture is merely placed over

the diffracted beam. But in a high resolution DF, the beam is tilted so that $-\underset{\sim}{g}$ instead of $\underset{\sim}{g}$ is the reflection responsible for contrast. Thus, the pseudo-complementary edge fringes in BF and DF respectively will occur where the fault plane intersects the top surface of the foil. The geometry of the fault plane, diffracting vector $\underset{\sim}{g}$ and displacement vector $\underset{\sim}{R}$ is given in Fig. 16. With this geometry, the fault is determined to be extrinsic since, the bottom part of the crystal is displaced away from the top part, necessitating the filling in of material. The formation of extrinsic faults can be thought of in this manner.

As with the closely spaced faults discussed previously, there is still the possibility that the displacement vector could be one of the a/6 $\langle 112 \rangle$ vectors in $(1\,\bar{1}\,\bar{1})$. To deduce whether these isolated faults are either growth or shear, the partials bounding the faults must be analyzed. No isolated fault, at this writing, has shown partial dislocations which have yielded to such an analysis.

B. Dislocations in β-SiC

1. Dislocation Dipoles

Results

Dislocations were observed in β-SiC occurring as dipole pairs with Burgers vector of the type $\pm$ a/2 $\langle 110 \rangle$. The dipole nature of the dislocations was determined by examining the symmetry of the contrast arising from the dislocation pair. This analysis will be explained in the following section. Figure 12 shows these dipoles

(marked D) in four reflections. For $20\bar{2}$ and $2\bar{2}0$, (Fig. 12a and c), they are visible. The dipoles are invisible (or have residual contrast for the reflections $2\bar{4}\bar{2}$ and $11\bar{1}$ in Figs. 12b and d.

Discussion

Dislocations associated together as dipoles have Burgers vectors differing only in their sign. The difference in sign of $\underset{\sim}{b}$, the Burgers vector, was indicated by the differing behavior of the light-dark oscillations occurring adjacent to the images of the dislocations comprising the pair. Figure 17a again shows the dislocation pairs when $\underset{\sim}{g} = 2\bar{2}0$. Observing the dislocation marked d_1, it is noted that the light-dark oscillations "bow-out" towards the right side of the image of the dislocation. For the dislocation marked d_2, the direction of bow-out is towards the left. It is noted, also, that dark oscillatory contrast occurs adjacent to similar dark contrast of the second dislocation. This behavior is indicated by the opposing arrows adjacent to d_1 and d_2 in Fig. 17a. The contrast from the dark-light oscillations, then have a line of symmetry lying halfway between and parallel with the dislocation pair. This line of symmetry is indicated in Fig. 17b by the two arrows between the same dislocations d_1 and d_2, for which (in the reflection $\underset{\sim}{g} = \bar{3}11$), the direction of bow-out of the oscillations is towards the "outside" of the dislocation pair.

It can be concluded then, that the Burgers vectors of the dislocations are opposite in sign and that the pairs of dislocations can be associated as dipoles. Other tests to determine the dipole nature of dislocation pairs are described by Bell, Roser, and Thomas.[27] The

width between the images of the dislocations changes when s, the deviation parameter changes sign, keeping $\underset{\sim}{g}$ constant. This test was not performed on the dipoles described.

In determining the Burgers vector of the dipoles, certain working assumptions were made. Since β-SiC is a covalently bonded material with an fcc type structure, the dislocations present in the material could most probably reside in the close packed {111} planes. This assumption was borne out by a trace analysis of the line directions in 3 different zones of the crystal. These orientations were [101], [112], and [111]. The line direction in these zones were respectively $[\bar{1}21]$, $[\bar{1}10]$ and $[\bar{1}10]$. The conclusion was that the dipoles lay along $[\bar{1}10]$, and that they occur on the $(11\bar{1})$ close packed planes.

The determination of $\underset{\sim}{b}$, their Burgers vector, involved difficulties associated with the striation contrast reported in Section V(A.1). In fact, Fig. 12a shows these dipoles (marked D) at the same time the striations are in contrast. Figure 12c shows the dipoles when the striations were absent. Only in those reflections for which the striations were invisible, was unhampered observation of the dipoles possible.

That the dipoles lay in the $(11\bar{1})$ planes, excluded them from being Frank dipoles with Burgers vectors $\pm$ 1/3$[11\bar{1}]$ since these would be visible when $g = 11\bar{1}$. Figure 12d shows them to be invisible in this reflection. The following table summarizes the contrast from the dipoles.

Table 2

$\mathbf{g}\cdot\underset{\sim}{b}$ Values for $\frac{a}{2}\langle 110\rangle$ Dislocations and Observed Contrast from Dipoles

Actual Contrast	$\mathbf{g}$	$\frac{a}{2}[101]$	$\frac{a}{2}[011]$	$\frac{a}{2}[1\bar{1}0]$	$\frac{a}{2}[10\bar{1}]$	$\frac{a}{2}[01\bar{1}]$	$\frac{a}{2}[110]$
Invisible	$11\bar{1}$	0	0	0	1	1	1
Visible	$\bar{3}11$	-1	1	-2	-2	0	-1
Visible	$2\bar{2}0$	1	-1	2	1	-1	0
Invisible	$2\bar{4}\bar{2}$	0	-3	3	2	-1	1

The Burgers vector was then determined to be $\frac{a}{2}[101]$ which is in 60° orientation with line direction of $[1\bar{1}0]$.

The dipoles observed and analyzed in this material are composed of pairs of glide dislocations on {111} planes. This fact points to the possibility that the dipoles were formed by plastic deformation at the sintering temperatures at which the compact was fabricated. Evidence for the glide of dislocations at high temperatures in MgO, a ceramic material of high melting point, was presented by Washburn, Kelly and Williamson in 1960.[28] High temperatures were obtained by deliberate beam current heating in the transmission microscope. Observation of dislocation structures in other ceramic materials show evidence for the formation of dipoles at high temperatures. Barber and Tighe[29] studied the structures developed in creep deformed specimens of aluminum oxide. The dislocations in their foils lay in well defined glide bands which contained dislocation loops and dipoles. Pletka, Mitchell, and Heuer[30] reported on the dislocations substructure developed in sapphire single crystals deformed at 1200°C to 1500°C. Different foils strained to different values were examined

and the substructure observed consisted, again, mainly of dipoles when the strain was that due to stresses between the upper and lower yield points.

2. Other Dislocations

Results

In addition to the dipoles, other dislocations were observed in β-SiC. The observation of these dislocations was not an isolated instance in the course of the investigation. An example of a grain exhibiting these dislocations is shown in Fig. 18a together with its corresponding diffraction pattern (18b). Figure 18a is a BF image taken looking down the [111] symmetric orientation as evidenced by the diffraction pattern. The dislocations of Fig. 18a were analyzed and their Burgers vectors were found to be $\pm \frac{a}{2}[101]$, $\pm \frac{a}{2}[011]$ or $\pm \frac{a}{2}[110]$. None of these Burgers vectors are found in the (111) plane perpendicular to the beam direction.

The diffraction patterns from these grains exhibited extra spots in the $\frac{1}{3}\langle 422\rangle$ type positions. These extra spots are observed in the diffraction pattern of Fig. 18b, one of which is pointed out by an arrow. Tilting alone a $\langle 220\rangle$ Kikuchi band from this [111] zone to a [112] zone, additional extra spots are observed. These are indicated in Fig. 19. The extra spots in this zone are in the $\frac{1}{2}\langle 113\rangle$ positions.

Discussion

Figure 20a again shows the dislocations first exhibited in 18a.

The distinctions between dislocations m and n are clarified in Fig. 20b and c. Figure 20b shows m visible and n invisible, while 20c shows the opposite--i.e., m, invisible, n visible. Analysis shows m to become invisible in $20\bar{2}$, $\bar{1}\,\bar{1}\,1$, and $1\,\bar{1}\,\bar{1}$ making its Burgers vector $\pm \frac{a}{2}$ [101]. n is invisible in $02\bar{2}$, $\bar{1}1\bar{1}$, and $\bar{1}\,\bar{1}\,1$ thus making its Burgers vector $\pm \frac{a}{2}$[011]. A similar analysis determines the Burgers vector for the following dislocations in Fig. 20a.

s: $\pm \frac{a}{2}$[101]

t: $\pm \frac{a}{2}$[011]

u: $\pm \frac{a}{2}$[110]

v: $\pm \frac{a}{2}$[101]

w: $\pm \frac{a}{2}$[110]

x: $\pm \frac{a}{2}$[011]

y: $\pm \frac{a}{2}$[011]

Dislocations m and n, for part of their lengths are closely associated spatially. In the bright field image of the [111] symmetric orientation, (Fig. 20a), the projections of m and n lie on top of each other before they diverge to become distinct dislocations. Figure 20d shows m and n in the reflection $2\bar{2}0$ where they are both visible. (A stereo pair showed m and n to lie one above the other).

The dislocations observed, which have Burgers vectors $\frac{a}{2}$[101], $\frac{a}{2}$[110], or $\frac{a}{2}$[011], are seen to form networks (see Figure 18a and 20a). Networks such as these, as with the dipoles, are dislocation structures

which plastic deformation are likely to produce at the high sintering temperatures under which this material was fabricated. Another possibility exists that the dislocation networks were present in the crystallites prior to sintering.

Attempts were made to ascertain the origin of the extra spots observed in the [111] and [112], zones. The [111] (fcc) zone, as described above, had extra spots in the $\frac{1}{3}\langle 422\rangle$ positions in the diffraction pattern. A construction of the second Laue layer of any reciprocal lattice zone is outlined by Hirsch et al (ref. 26, pp. 114-115). Using this procedure, the effect of a second Laue layer in the [111] zone was determined. $\frac{1}{3}\langle 422\rangle$ type was determined. $\frac{1}{3}\langle 422\rangle$ type spots could originate from such an effect. But the effect of a second Laue layer giving rise to extra spots in the [112] zone was investigated and the result was negative. The conclusion was that the Laue layer effect, alone, could not explain the origin of the extra spots.

At this point, other crystal structures were posed for further attempts to explain the extra spots. Since hexagonal and rhombohedral polytypes are commonly observed in SiC formed by other processes, the most common polytypes--2H, 6H and 15R were chosen as candidates for investigation.

The [0001] zone of hexagonal and rhombohedral polytypes appear similar. Figure 21 shows indexed diffraction patterns from the [111] (fcc) zone and the [0001] (hexagonal) zone. The [111] and [0001] zones of cubic and hexagonal forms of SiC have indistinguishable electron diffraction patterns. A measured camera length of 23.83 mm Å gives a length of 15.5 mm for the $\langle 220\rangle$ type spots in the [111] fcc zone and

15.49, 15.51, and 15.50 mm, respectively for the 2H, 6H, and 15R polytypes. The length observed on the diffraction patterns were 15.5 mm ± 0.1 (the polytypes examined have the following c_o - and a_o - axis values: 2H: c_o = 5.048Å, a_o = 3.076Å; 6H: c_o = 15.079Å, a_o = 3.073Å; 15R: c'_o = 37.70Å, a'_o = 3.073Å.[7] The possibility that the grain was either Si or B_4C was considered. But the ⟨220⟩ spots for Si have length of 12.04 mm (λL = 23.83 mmÅ) and the ⟨11$\bar{2}$0⟩ spots are 8.51 mm long for rhombohedral B_4C with the given camera length. The possibility that the extra spots are actually ⟨11$\bar{2}$0⟩ type spots from a hexagonal crystal structure is ruled out, since the measured lengths of the extra spots from the transmitted beam is 9.20 mm, while at the camera length in operation, ⟨11$\bar{2}$0⟩ spots from hexagonal structures would be ~15.5 mm, as measured from the transmitted beam.

An attempt was made to ascertain whether the diffraction pattern of the [112] zone, together with the extra spots could originate from the crystal structure of the 2H, 6H, or 15R polytypes. This, too, proved fruitless.

Having exhausted reasonable possibilities for alternative crystal structures, other possibilities for exploring the extra spots were attempted. Double diffraction was ruled out since the extra spots occurred at $\frac{1}{3}$ ⟨422⟩ and $\frac{1}{2}$ ⟨113⟩, which are fractional multiples of allowed reflections. Such multiples sometimes occur for structures which undergo ordering involving more than one unit cell. This phenomenon, then, is manifested by the appearance of these spots corresponding to fractional indices which can be made integral by doubling if halves are involved and tripling, if thirds appear, etc. This

means that the unit cell in real space is twice or three times as large in these two cases in which case a superlattice is said to be present in the structure.

A dark field image using the $\frac{1}{2}$ $[1\bar{1}\bar{1}3]$ extra spot is shown in Fig. 22. In it we observe, in weaker contrast, the dislocations imaged in Fig. 20a. Dislocations w and y are shown again. Whether this micrograph shows evidence for ordered domains remains an unanswered question. The origin of the prominent "paint-brush" contrast, roughly parallel to $\underset{\sim}{g}$ needs to be explained and correlated with the possibility of a superlattice.

Section VI

CONCLUSION

This investigation of intra-granular defects in β-SiC by transmission electron microscopy has identified the presence of heavy faulting, isolated extrinsic faults, dislocation dipoles and dislocation networks the dipoles and other dislocation lines are most likely to have been formed during high temperature deformation. A possibility remains that some of the dislocation networks were comprised of grown-in dislocations that were present in the crystallites before sintering.

Suggestions for Future Work

The nature of the closely spaced faults is not completely determined. Since partial dislocations bounding the edges of these faults have not been observed, the question whether the faults are growth or shear type is still unanswered. Answering this question will involve the investigation of the $\beta \rightarrow \alpha$ SiC solid state transformation. Annealing experiments to observe what happens to these faults with heating above the transformation temperature may help in determining the nature of the faults.

High temperature deformation experiments can be performed to determine what role the dipoles and the other dislocations may play in the plastic behavior at these temperatures.

ACKNOWLEDGMENTS

I wish to express my gratitude to Professor Gareth Thomas for his guidance during the course of this research. I gratefully acknowledge the critical analysis of the thesis by Professor Jack Washburn. To Dr. David R. Clarke, I wish to express my appreciation for patient supervision and helpful discussions during the past two years. To Raja K. Mishra, Ronald Gronsky, Dr. Kenneth Westmacott, Dr. H. Peter Karnthaler, and Ulrich Dahmen, I also wish to express my thanks for helpful discussions.

To D. J. Pielech and Connie Calica I extend my appreciation for the typing of the thesis. A special thanks to Gloria Pelatowski for her reproduction of the line drawings.

To my mother and father, go my heartfelt gratitude and appreciation. For much needed respite and warmth, special thanks goes to my sister and friend, Celine Pornaras. I wish to express my gratitude to Janice Doty for her friendship and enduring support. And to Carolyn Leahy, I express my appreciation for special sustenance and a refreshing irreverent view of life.

The author expresses gratitude to the IBM Corp. for a fellowship during the academic year 1974-1975.

This research was performed under the auspices of the Energy Research and Development Administration through the Lawrence Berkeley Laboratory.

REFERENCES

1. R. J. Bratton, A. N. Holden in Ceramics for High Performance Applications, Burke, Gorum, Katz (eds.) p. 38, Brook Hill Publishing Company (1974).

2. S. Prochazka, Sintering of Dense Silicon Carbide, Report No. 74CRD067, Technical Information Series, General Electric Co. (1974).

3. A. F. Wells, Structural Inorganic Chemistry, Oxford University Press (1950).

4. G. S. Zhdanov and Z. V. Minervina, J. Phys. Moscow, 10 (1946) 422.

5. R. S. Mitchell, Z. Kristallogr. 109 (1957) 1.

6. L. S. Ramsdell, Amer. Mineral. 32 (1947) 64.

7. A. R. Verma and P. Krishna, Polymorphism and Polytypism in Crystals, pp. 83-88, Wiley (1966).

8. P.T.B. Shaffer, Acta Cryst. B25 (1969) 477.

9. A. H. Gomes de Mesquita, J. Cryst. Growth, 3 (1968) 747.

10. R.W.G. Wyckoff, Crystal Structures, Vol. I, Interscience (1963).

11. J. P. Hirth, J. Lothe, Theory of Dislocations, p. 354-355, McGraw-Hill Book Co. (1968)

12. J. Hornstra, J. Phys. Chem. Solids, 5 (1958) 129.

13. D. B. Holt, J. Phys. Chem. Solids, 23 (1962) 1353.

14. R. Stevens, J. Mat. Sci., 5 (1970) 474.

15. R. Stevens, J. Mat. Sci., 6 (1970) 324.

16. R. Stevens, J. Mat. Sci., 7 (1972) 517.

17. Bartlett and Martin, J. Appl. Phys., 39 (1968) 2324.

18. L. I. Van Torne, J. Appl. Phys., 37 (1966) 1849.

19. J. Cromer, Mat. Res. Bull., 4 (1969) 279.

20. T. D. Gulden, J. Amer. Ceram. Soc. 54[10] (1971) 498.

21. Van Landuyt and Amelinckx, Mat. Res. Bull. 6 (1971) 613.

22. Drum, Phys. Stat. Sol. 9 (1965) 635.

23. M. Yessik, S. Shinozaki, H. Sato, Acta Cryst., A31 (1975) 764.

24. P. Worthington, J. Mat. Sci. 8 (1973) 1194.

25. D. R. Clarke, G. Thomas, Proc. Elec. Mic. Soc. of Amer., 1976, September Meeting, Miami, Claitors (1976).

26. P. B. Hirsch, A. Howie, R. B. Nicholson, D. W. Pashley, M. J. Whelan, Electron Microscopy of Thin Crystals, pp. 222 ff. Butterworths (1965).

27. W. Bell, R. Roser, G. Thomas, Acta. Met. 12 (1964) 1247.

28. J. Washburn, A. Kelly, G. K. Williamson, Phil. Mag. 5 (1960) 192.

29. D. J. Barber and N. J. Tighe, Phil. Mag. 11 (1965) 495.

30. Pletka, Mitchell, Heuer, J. Amer. Ceram. Soc. 57 (1974) 388.

FIGURE CAPTIONS

Fig. 1 A single layer of SiC tetrahedra (from Shaffer, Acta. Cryst.[8]).

Fig. 2. (a) Parallel stacking of SiC tetrahedra, (b) Antiparallel stacking of tetrahedra (from Shaffer Act. Cryst.[8]).

Fig. 3. The unit cell of β-SiC(after F. P. Bunday, Scientific American, p. 66, Aug. 1974.)

Fig. 4. The β-SiC lattice projection normal to $(1\bar{1}0)$. Circles represent atoms in the plane of the paper; plus signs, those in the plane below. (111) is perpendicular to the plane of the paper and is seen as a horizontal trace (after Hirthe and Lothe[11]).

Fig. 5. (a) Intrinsic, I and (b) Extrinsic, E, faults in a projection normal to $(1\bar{1}0)$ (after Hirthe and Lothe[11]).

Fig. 6. (a) The β-SiC structure, [111] vertical. The black spheres represent silicon atoms and the white spheres, carbon atoms. The dashed line represents a (111) slip plane, with the line direction $\underset{\sim}{a}$ and the Burgers vector $\underset{\sim}{b}$ of a 60° dislocation shown. (b) The arrows indicate the result of moving the 60° dislocation from right to left (c) The rejoining of bonds after the dislocation has moved produces the 60° dislocation in β-SiC. $\underset{\sim}{a}$ and $\underset{\sim}{b}$ are along ⟨110⟩ directions and the slip plane is of {111} type.(after Holt, J. Phys. Chem. Solids[13]).

Fig. 7. The 60° dislocation in sphalerite structures seen in a projection normal to $(10\bar{1})$ and also showing the two possible

types of slip planes discussed in the text (after A. Kelly, G. Groves, Crystallography and Crystal Defects, Addison Wesley (1970)).

Fig. 8. 60° dislocation in sphalerite structure, Type I slip plane (after Hirthe and Lothe[11]).

Fig. 9. A scanning electron micrograph of the etched surface of β-SiC showing the grain size of approximately 10 μm.

Fig. 10. A transmission electron micrograph (100 kV) of a heavily faulted grain in β-SiC.

Fig. 11. (a) Lower magnification micrograph (100 kV) of the heavily faulted grain of Fig. 10 showing, in the circled area, the edge on $(\bar{1}\,\bar{1}\,1)$ faulted planes, as well as dislocation dipoles, pointed out by the arrow. (b) The electron diffraction pattern from this area showing streaking due to the faulting and extra spots (arrow) due to periodic faulting.

Fig. 12. Faulting visible in (a) becomes invisible in (b), (c), (d) Dislocation dipoles D visible in (a), (c); residual contrast in (b); invisible in (d). (100 kV)

Fig. 13. Area in β-SiC (100 kV) showing overlapping stacking faults P and an isolated fault F, chosen for analysis (see text).

Fig. 14. A stacking fault in β-SiC visible in (a) when $\underset{\sim}{g} = 1\bar{1}1$, invisible in (b) $\underset{\sim}{g} = 1\,\bar{1}\,\bar{1}$, (c) $\underset{\sim}{g} = 02\bar{2}$, and (d) $\underset{\sim}{g} = \bar{1}\,\bar{1}\,3$. The disappearances are consistent with the fault having a displacement vector $R = +\frac{1}{3}[1\,\bar{1}\,\bar{1}]$ (100 kV).

Fig. 15. A BF-DF pair of images for fault F (a) showing dark edge fringes indicating that $\alpha = -2\pi/3$ and (b) DF asymmetry for the edge fringes indicating the inclination of the fault with respect to the foil plane (see text) (100 kV).

Fig. 16. A schematic diagram showing the relationships between $\underset{\sim}{g}$ $\underset{\sim}{R}$, and the fault plane to give an extrinsic fault.

Fig. 17. (a) Dislocation dipoles showing symmetrical oscillatory contrast towards the "inside" of the pairs (arrows) and (b) towards the "outside" of the pairs. Arrows indicate line of symmetry for the oscillatory contrast. (100 kV)

Fig. 18. (a) Dislocation network β-SiC, [111] symmetric orientation, (b) Diffraction pattern: [111] zone (100 kV), extra spots in $\frac{1}{3}\langle 422\rangle$ positions, one pointed out by the arrow.

Fig. 19. The [112] zone (100 kV) with extra spots in the $\frac{1}{2}\langle 113\rangle$ positions (arrow).

Fig. 20. Electron micrographs, (100 kV), showing dislocations in β-SiC under various diffracting conditions. (a) [111] symmetric orientation, (b) $\underset{\sim}{g} = 02\bar{2}$, (c) $\underset{\sim}{g} = 20\bar{2}$, (d) $\underset{\sim}{g} = 2\bar{2}0$.

Fig. 21. Electron diffraction spot patterns for (a) the [111] face-centered cubic zone (b) [0001] hexagonal zone.

Fig. 22. DF image using $\frac{1}{2}[\bar{1}\,\bar{1}\,3]$ extra spot for imaging. (100 kV)

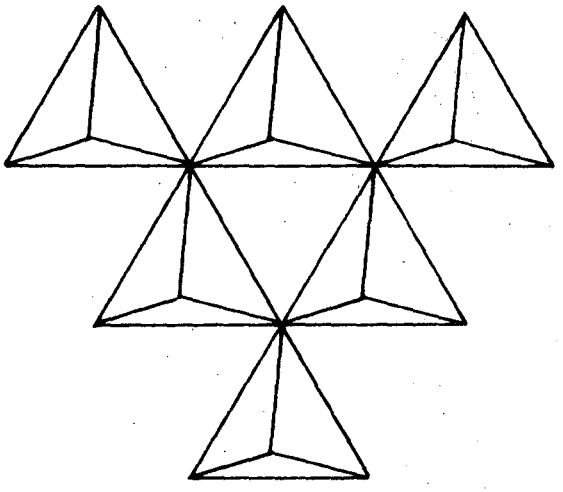

XBL 767-7171

FIGURE 1

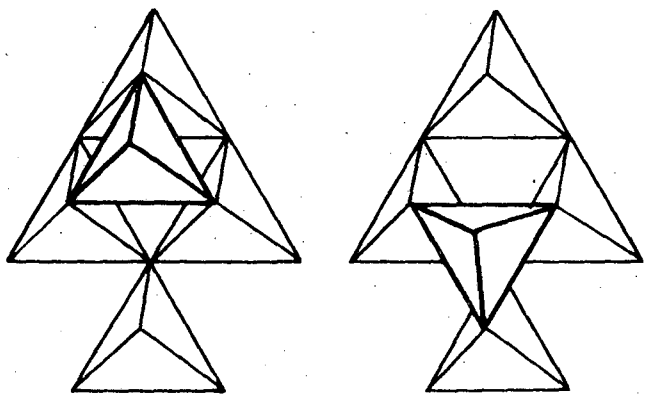

FIGURE 2

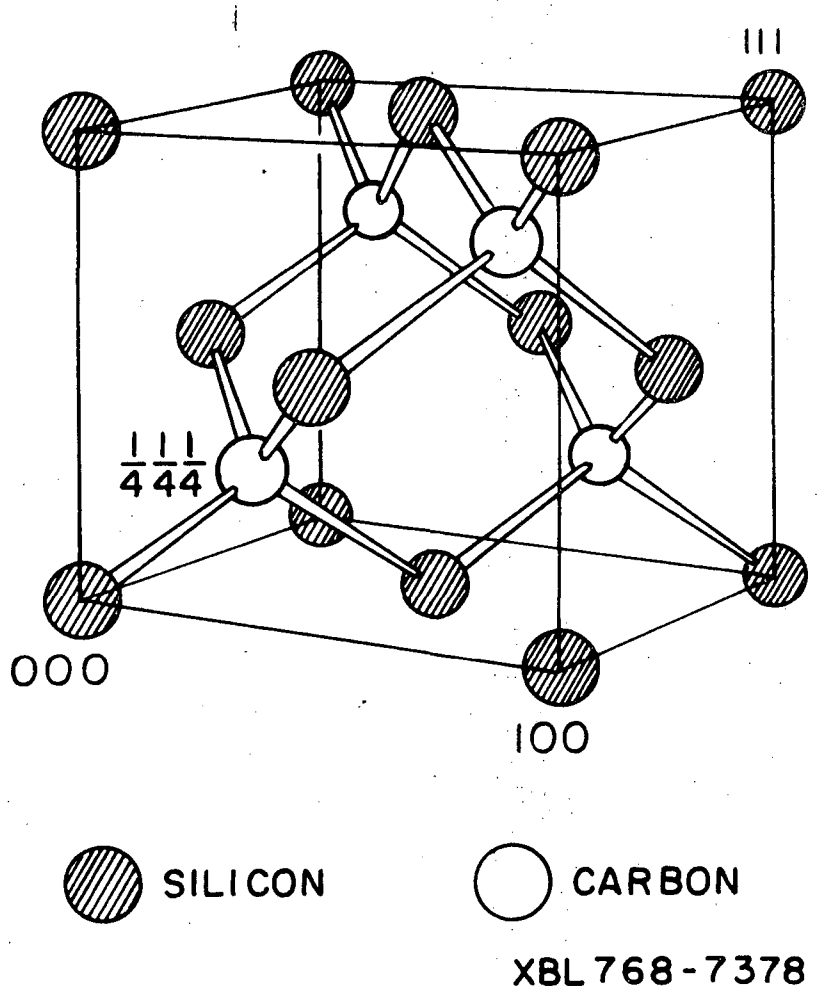

FIGURE 3

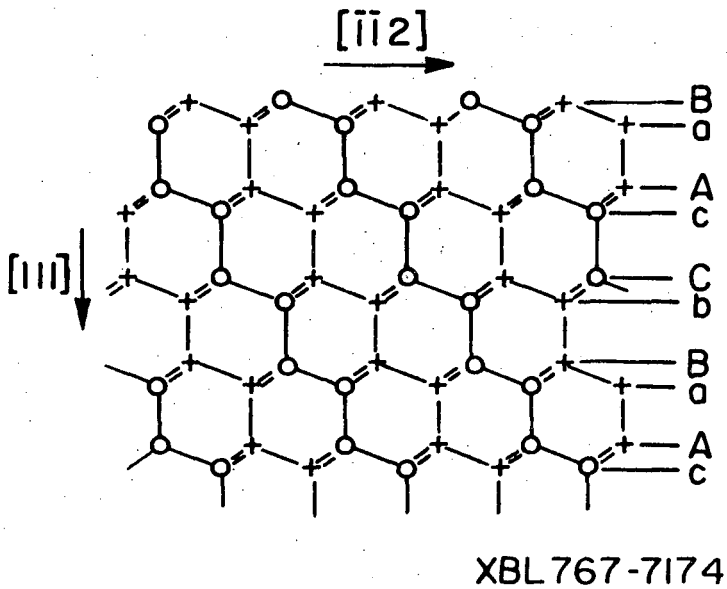

FIGURE 4

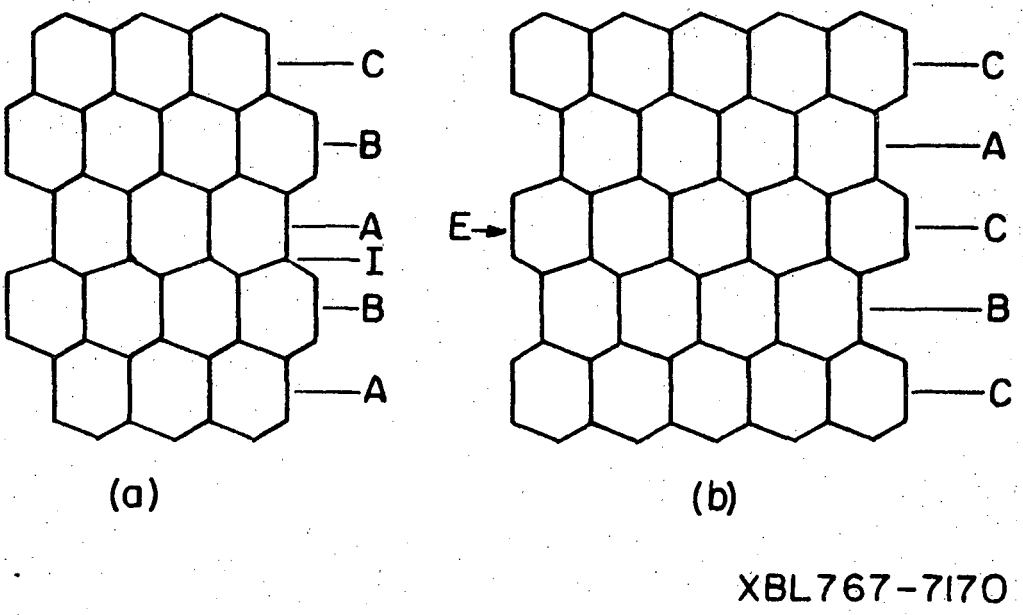

FIGURE 5

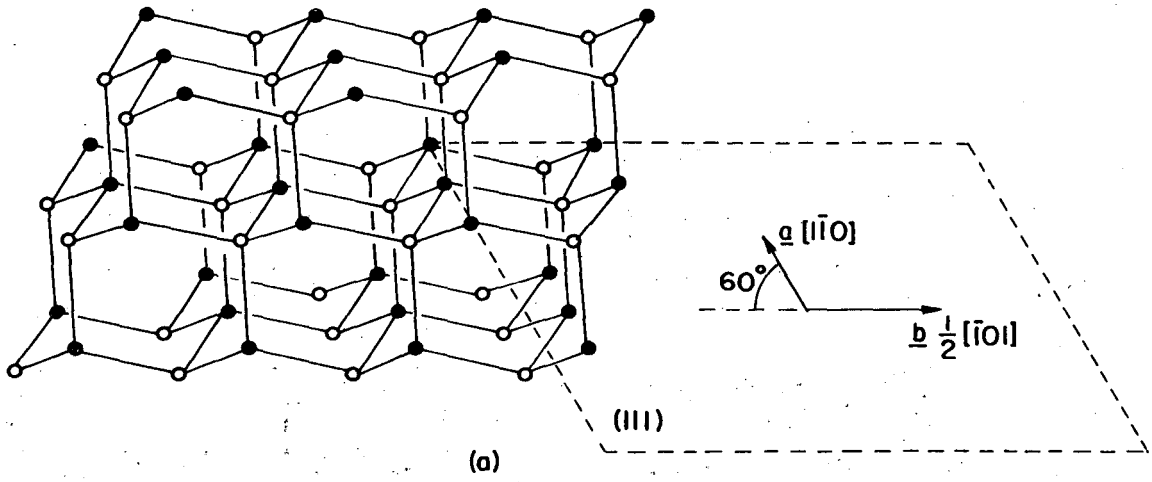

(a)

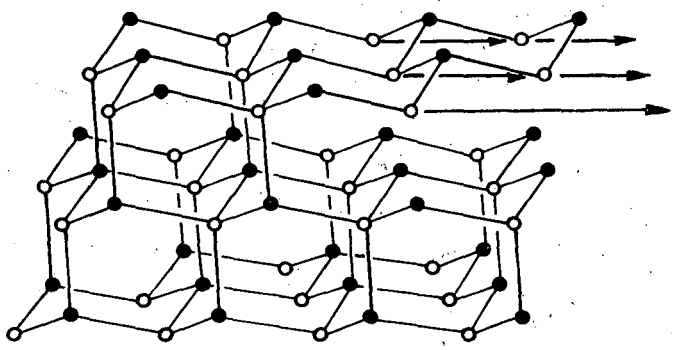

(b)

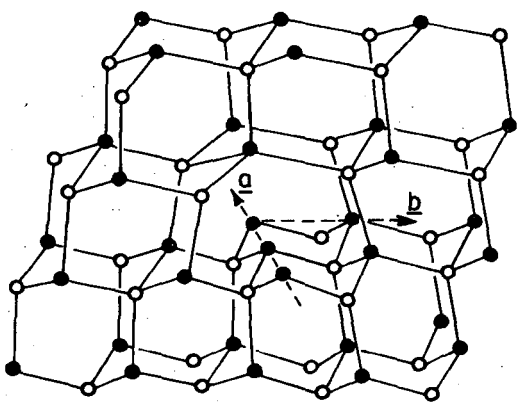

(c)

XBL 768-7379

FIGURE 6

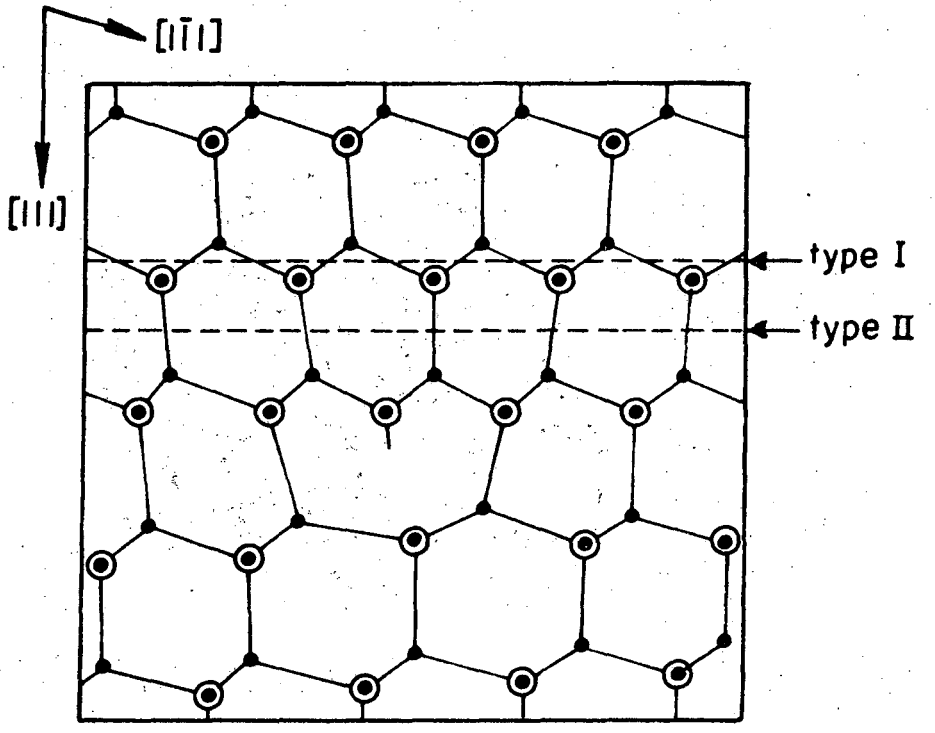

XBL 767-7173

FIGURE 7

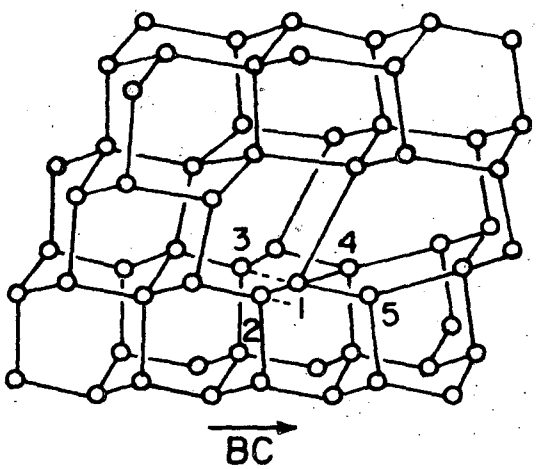

XBL 767-7175

FIGURE 8

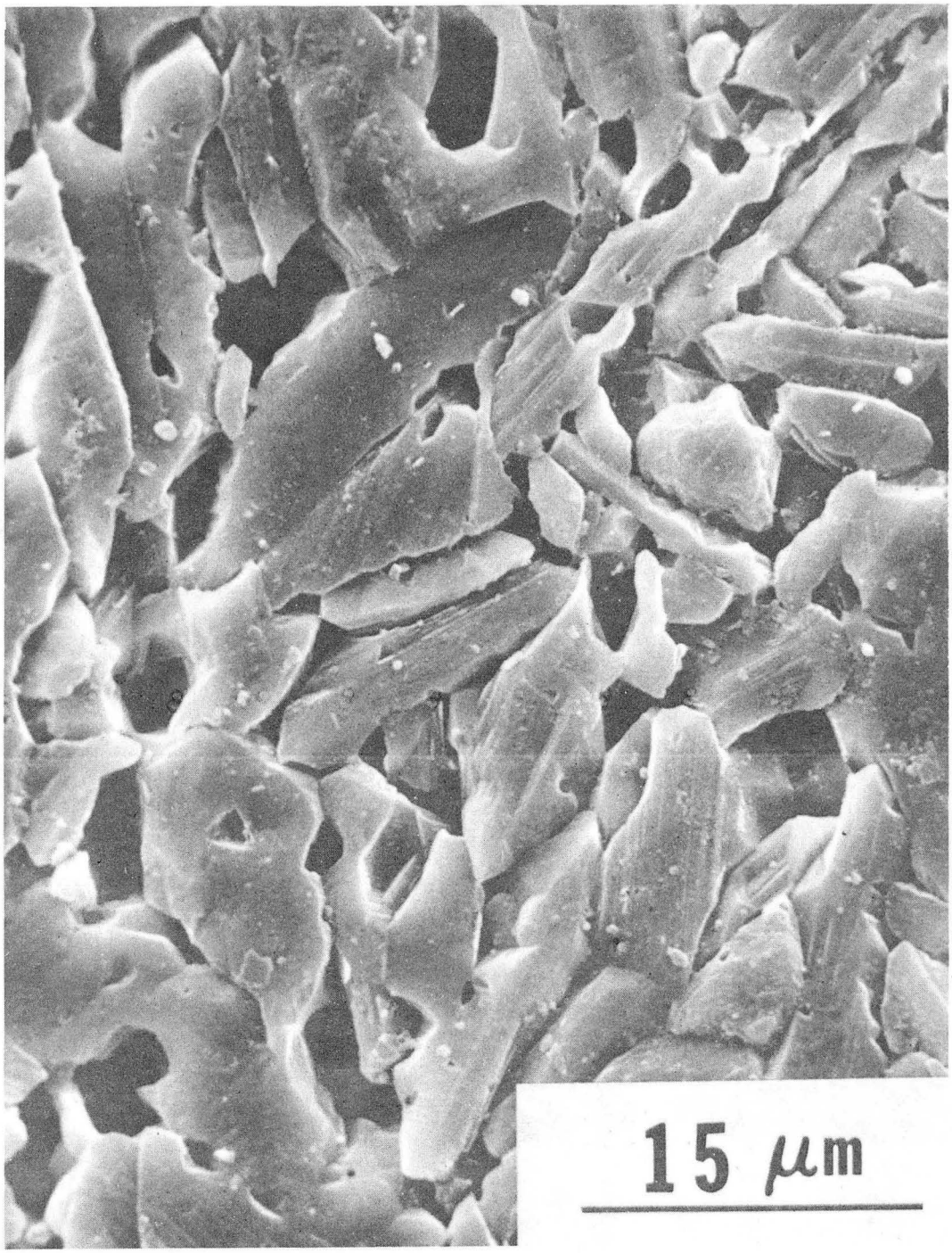

XBB 760-10542

FIGURE 9

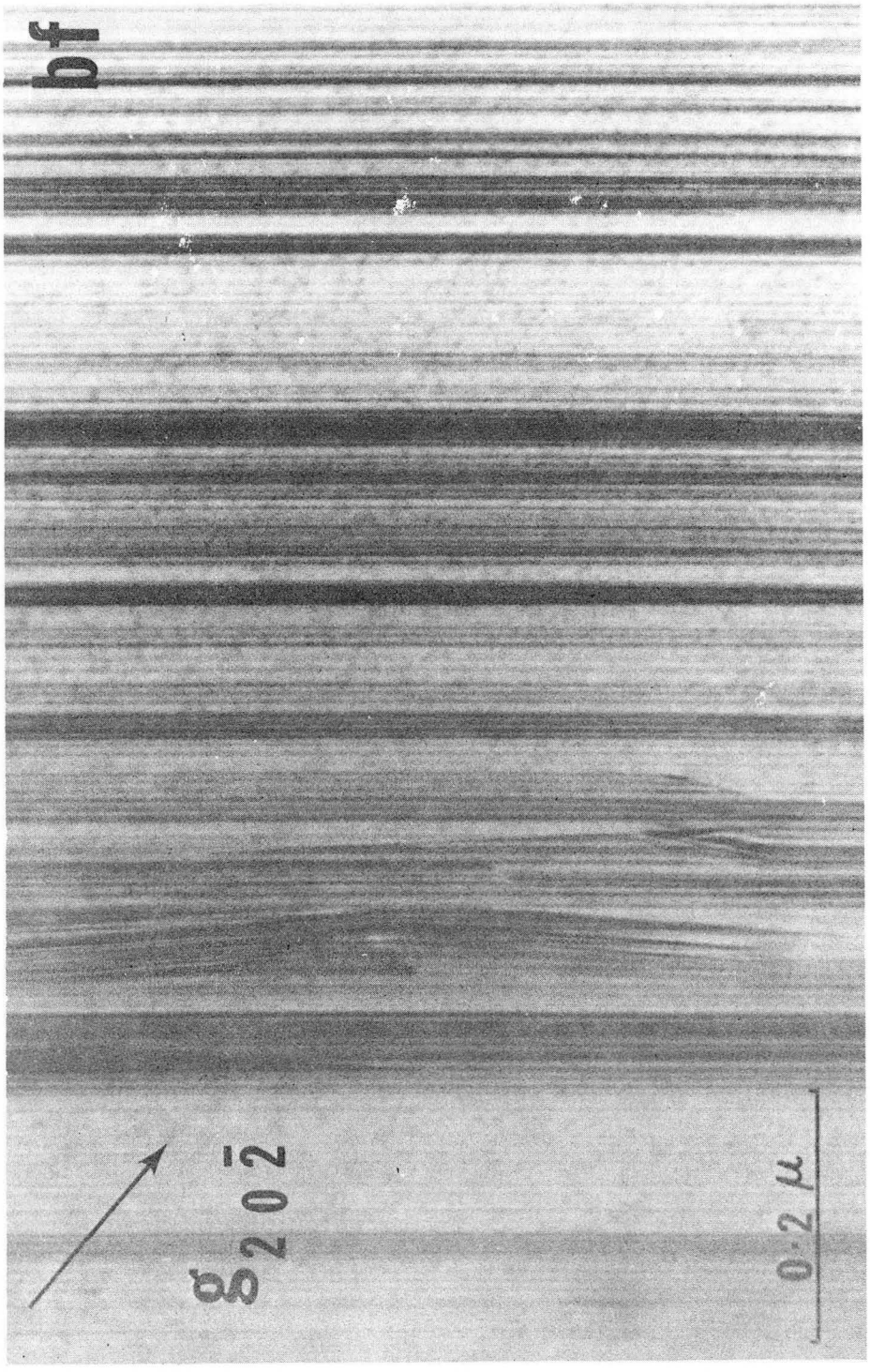

XBB 760-10540

FIGURE 10

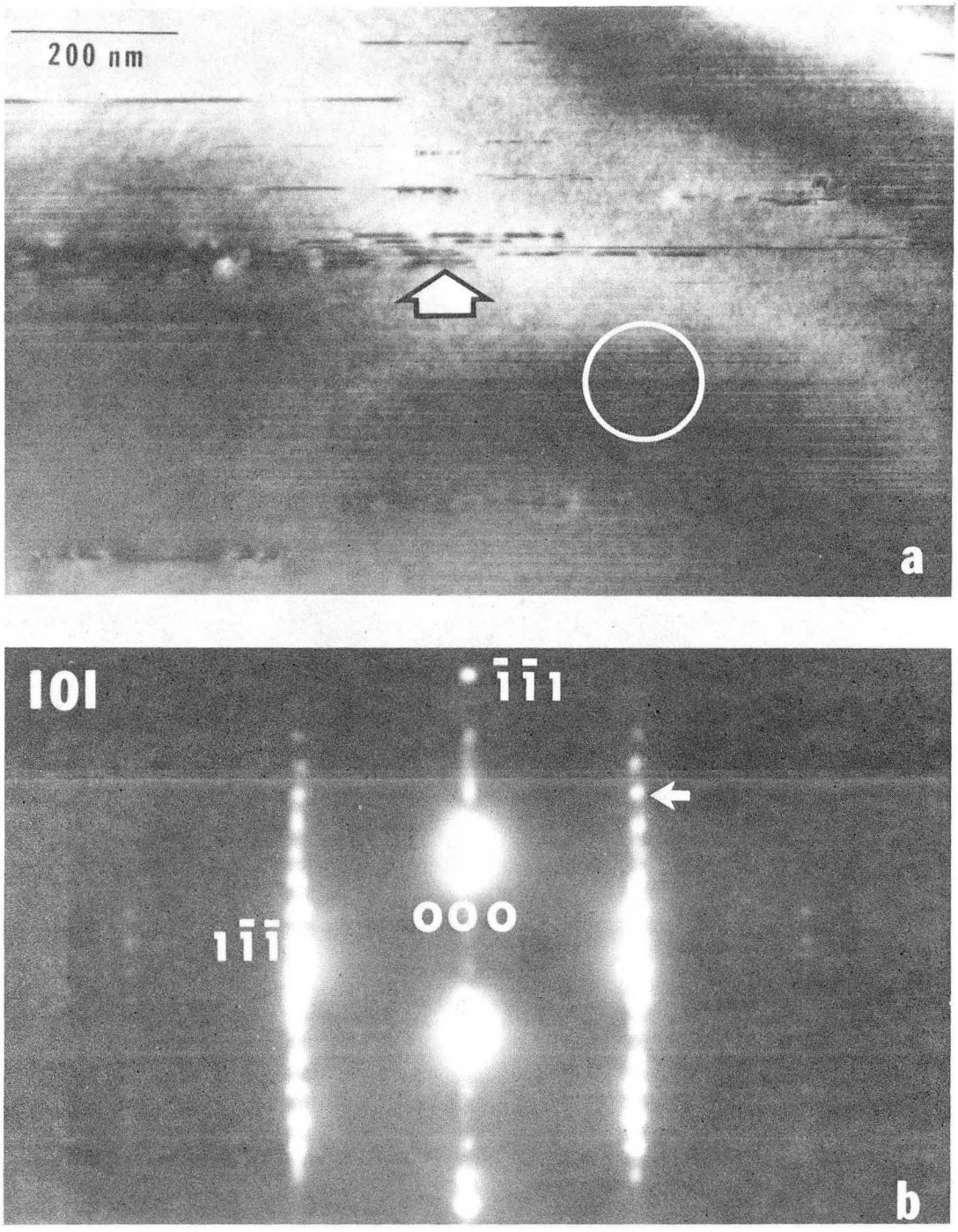

XBB 760-10539

FIGURE 11

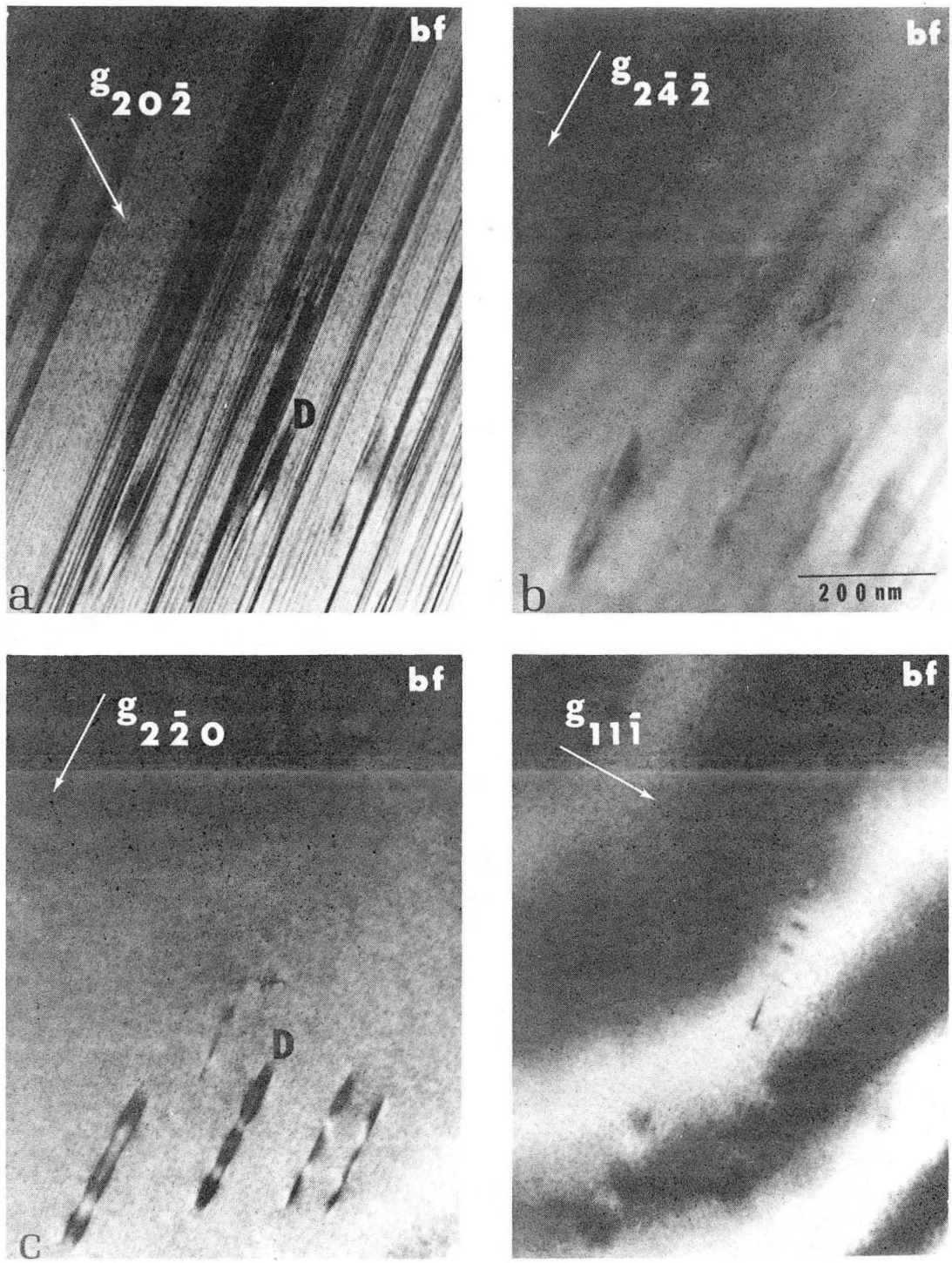

XBB 7610-9881

FIGURE 12

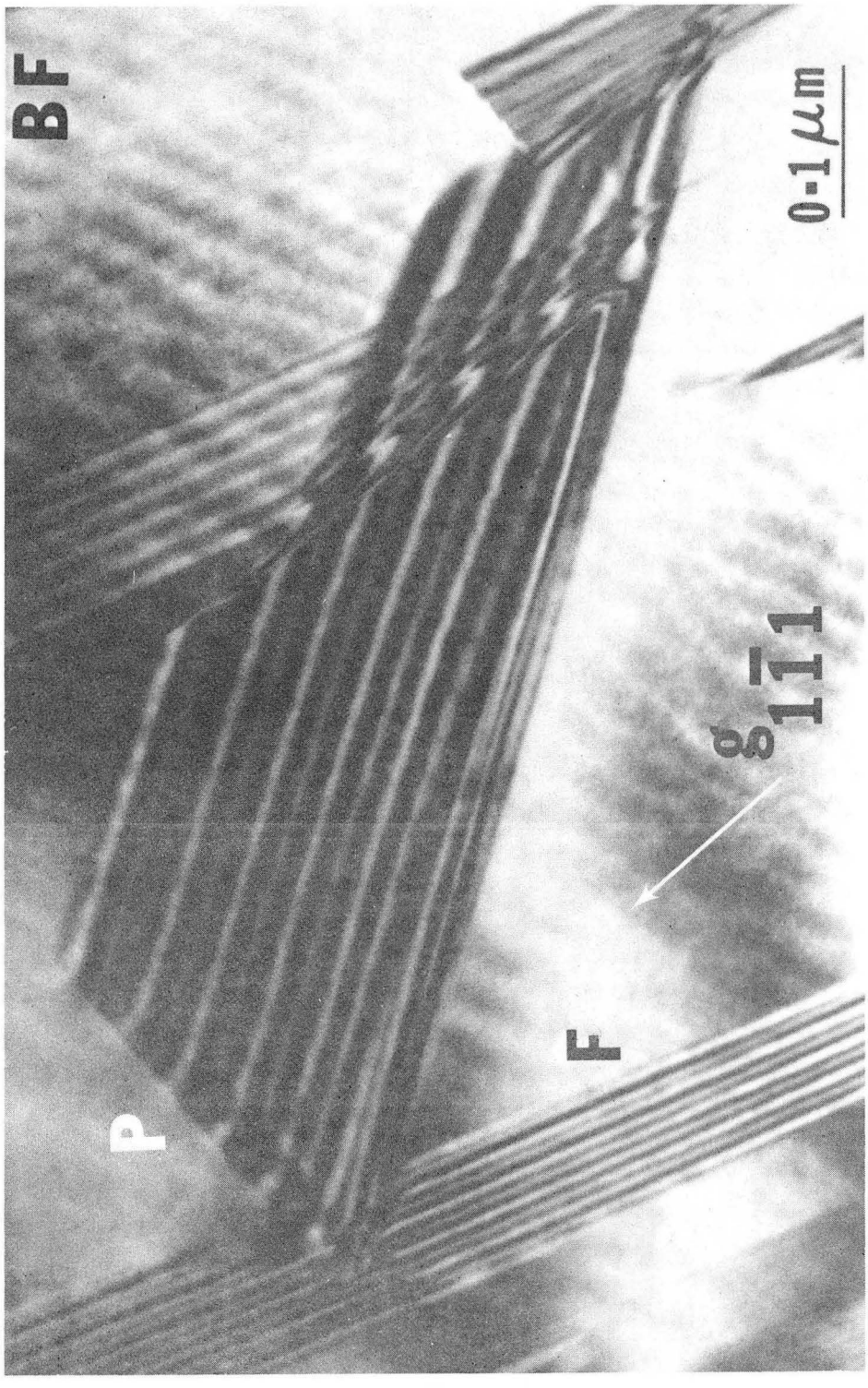

XBB 760-10541

FIGURE 13

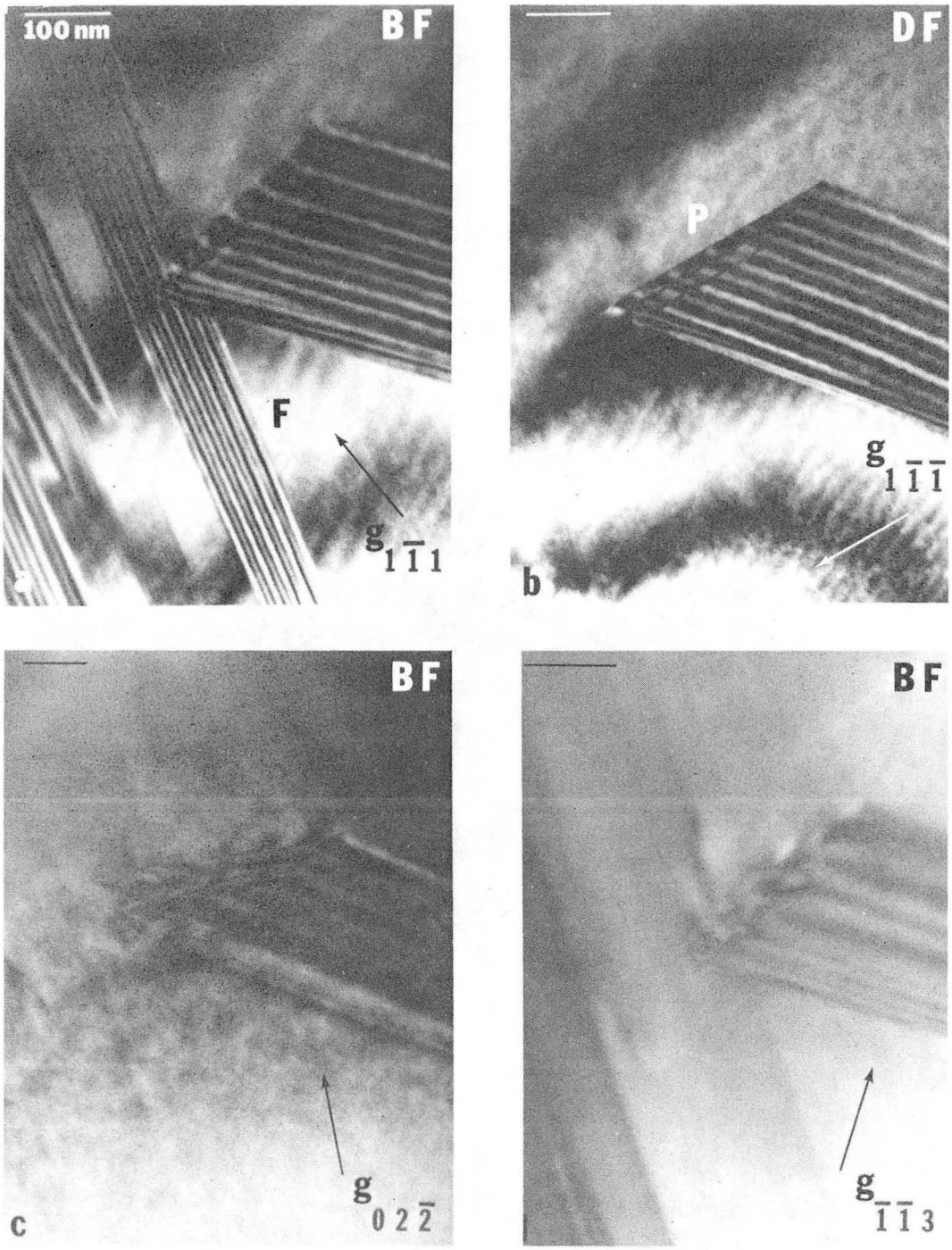

XBB 760-10535

FIGURE 14

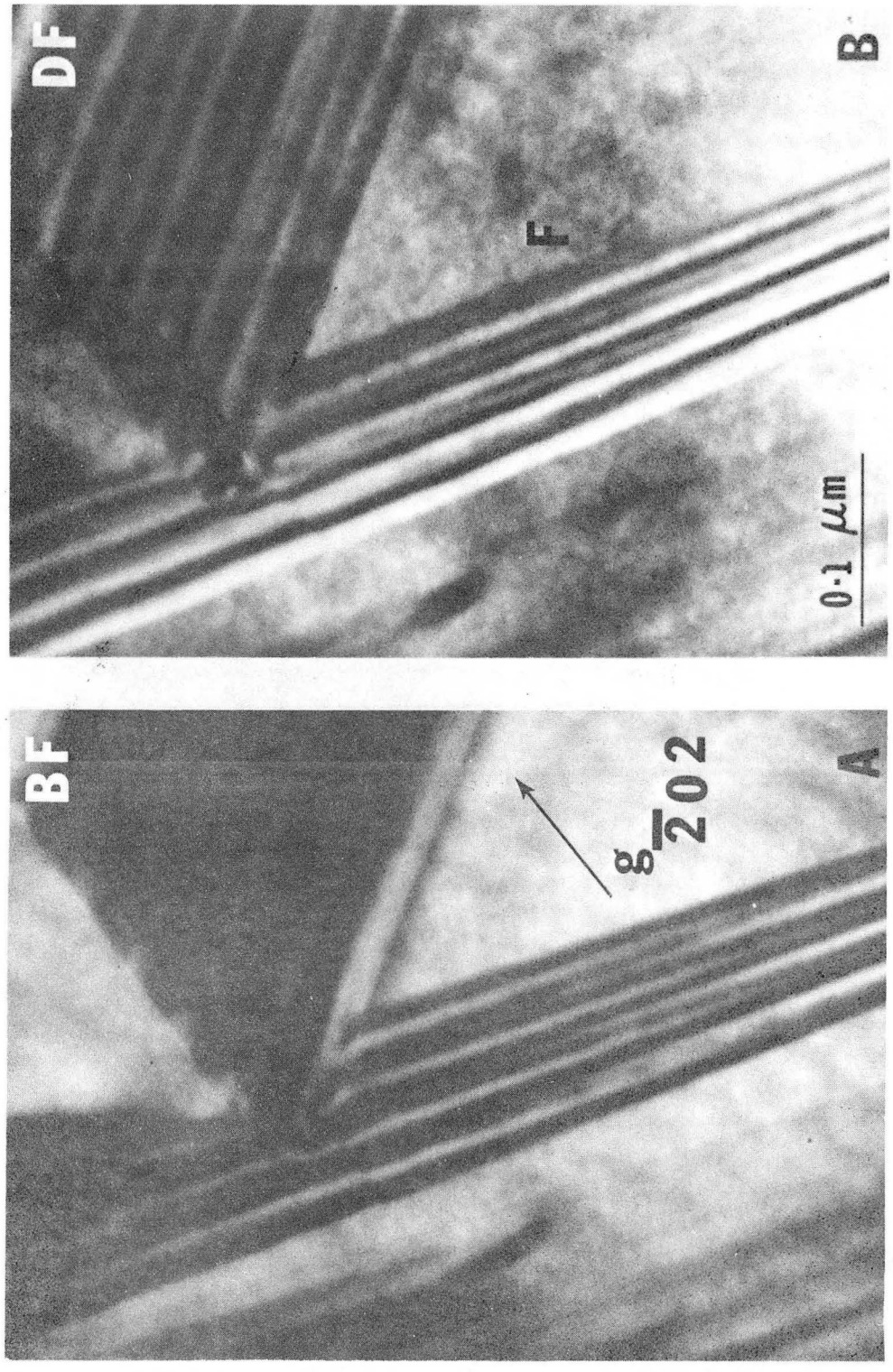

XBB 760-10537

FIGURE 15

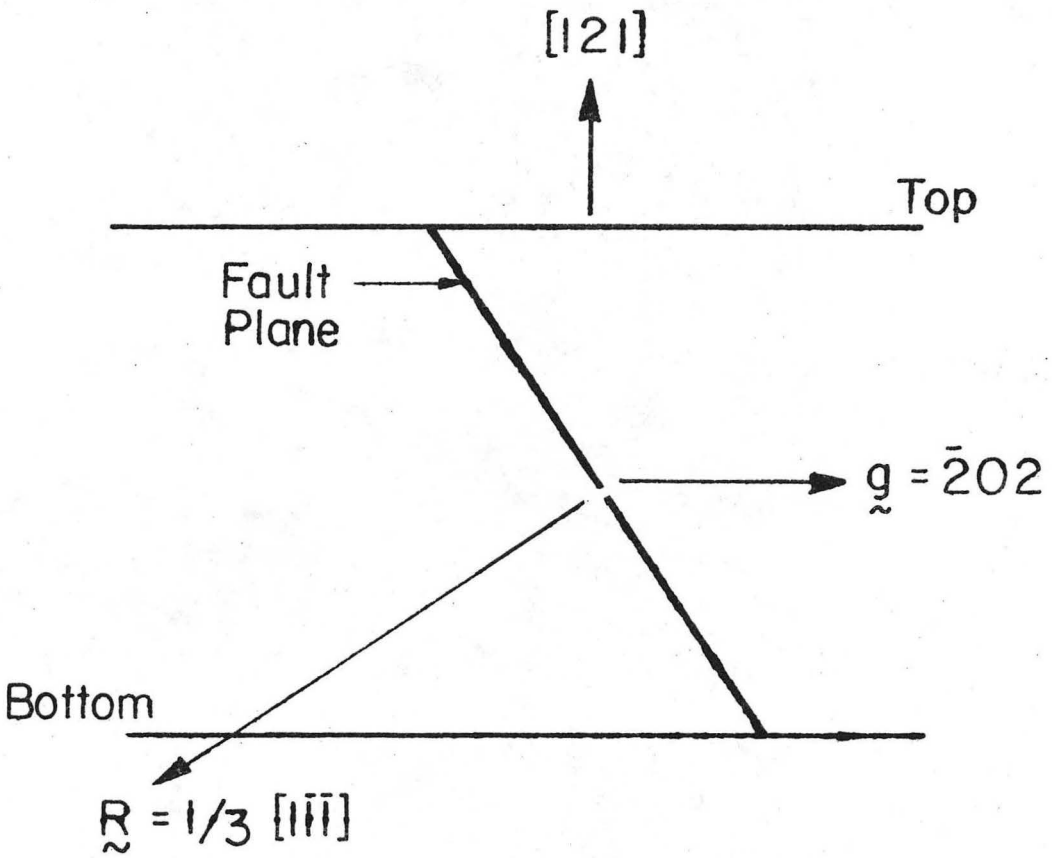

FIGURE 16

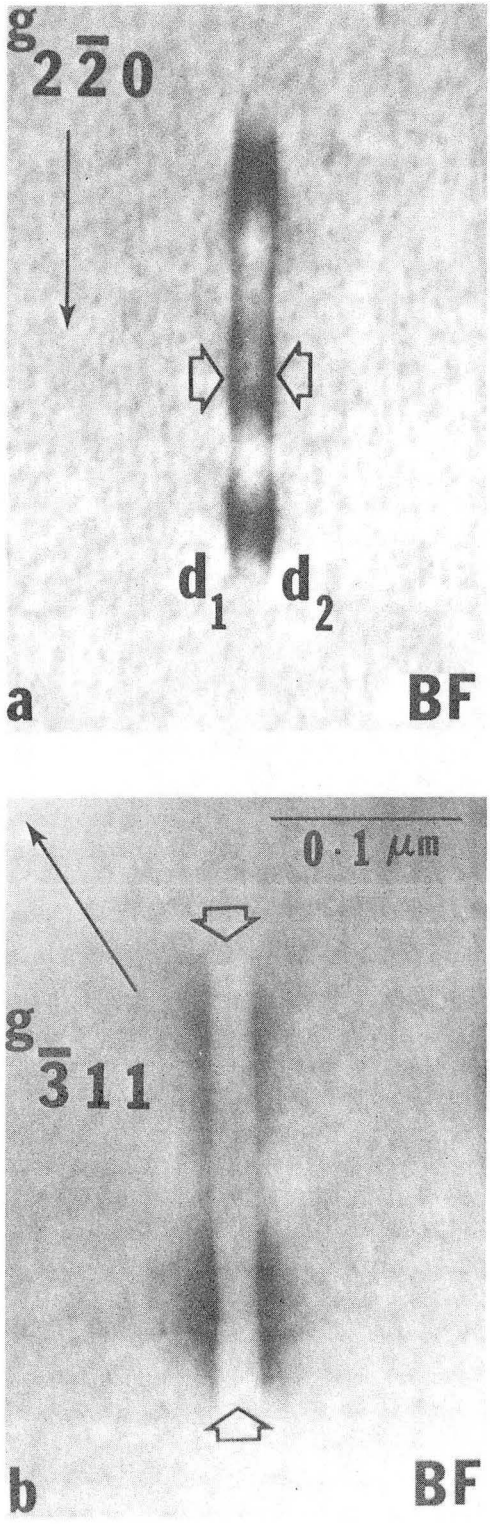

XBB 760-10536

FIGURE 17

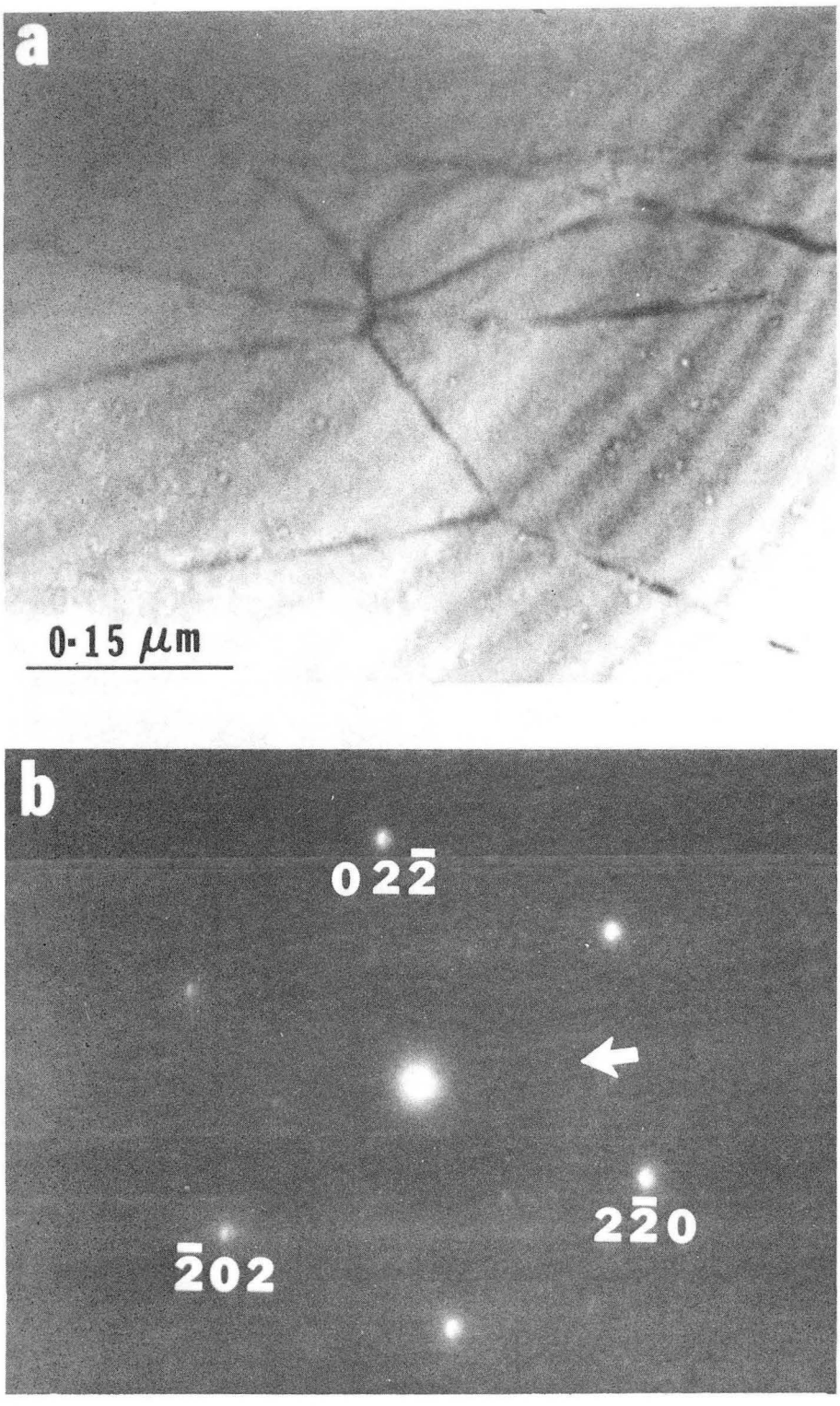

XBB 760-10534

FIGURE 18

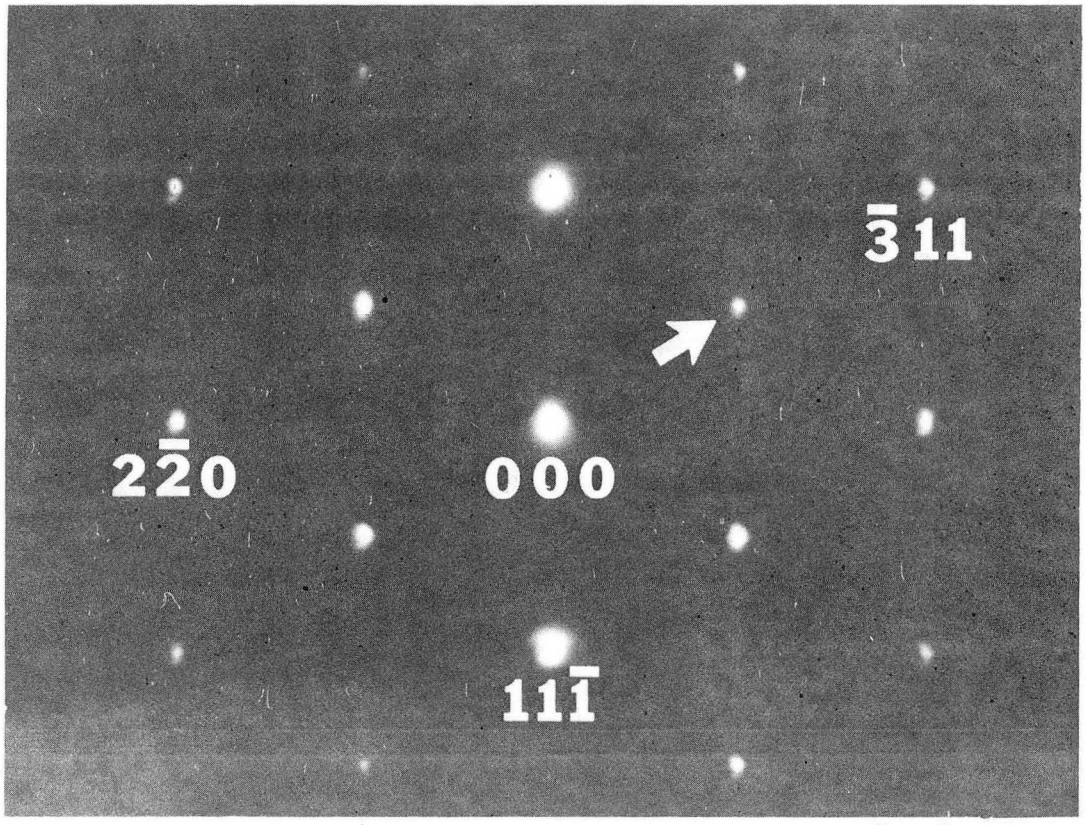

XBB 760-10544

FIGURE 19

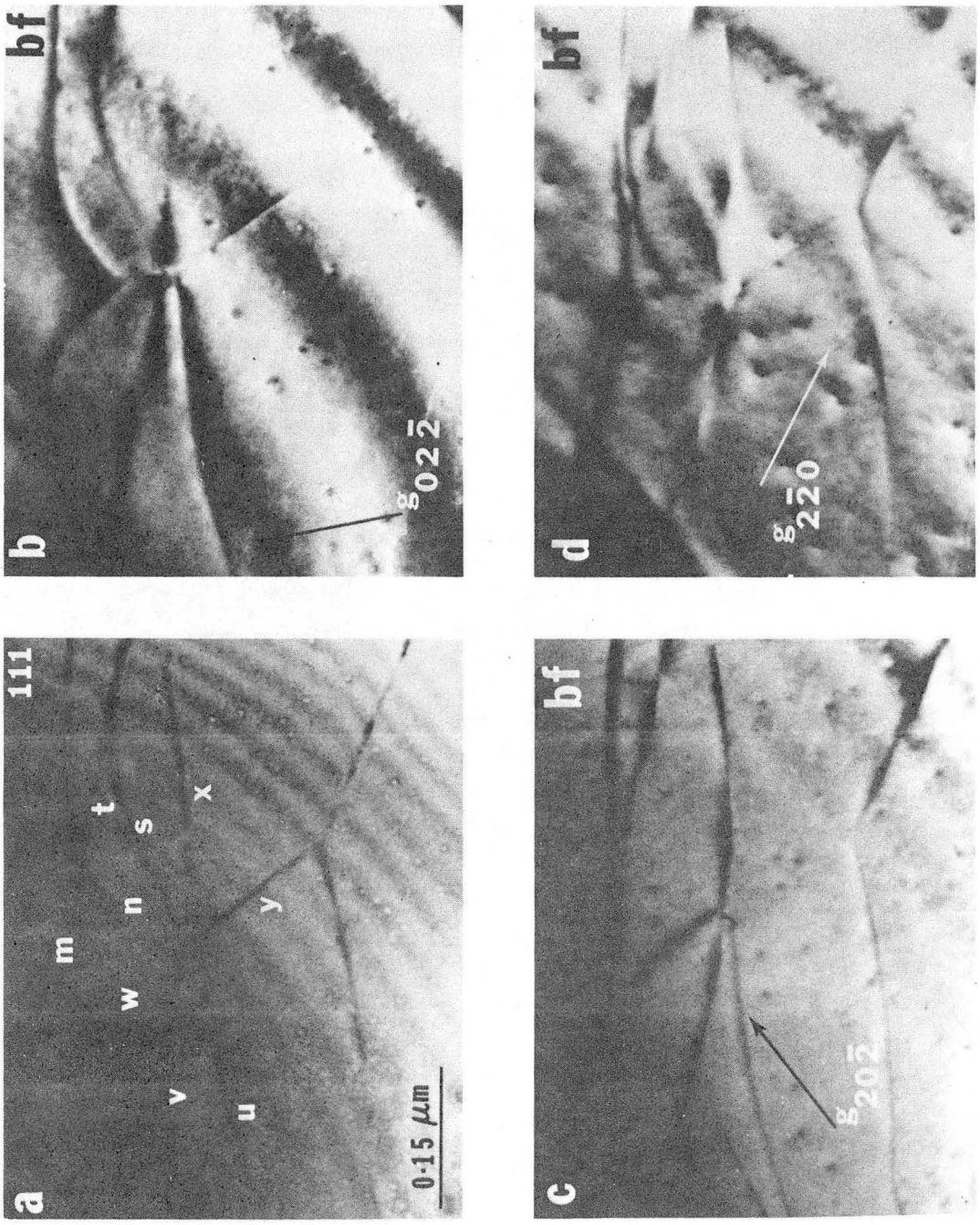

XBB 760-10539

FIGURE 20

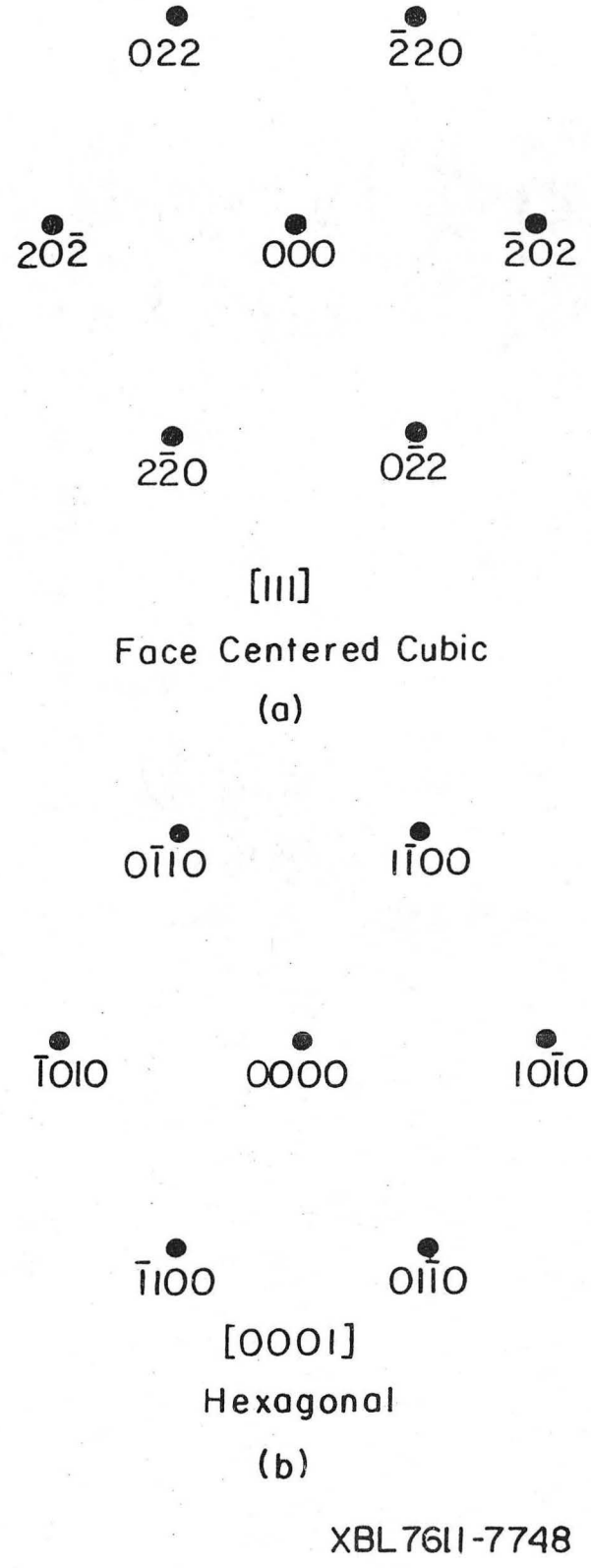

FIGURE 21

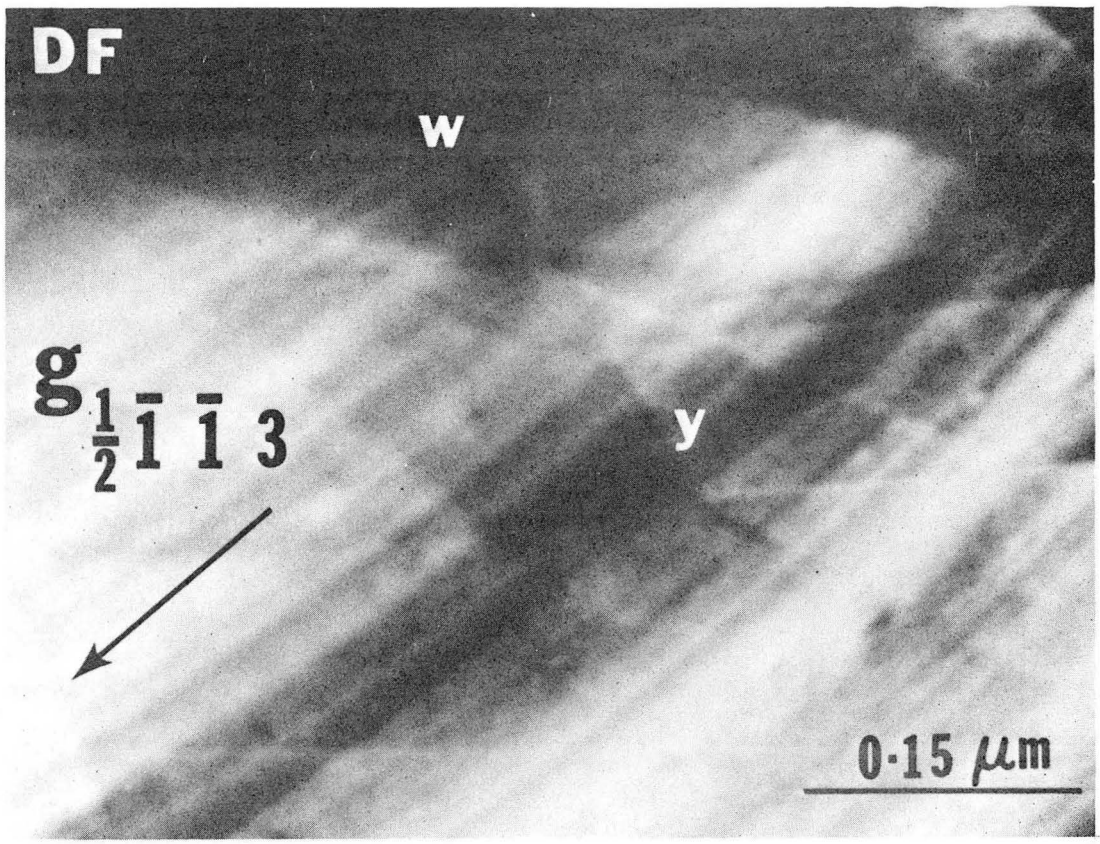

XBB 760-10543

FIGURE 22

This report was done with support from the United States Energy Research and Development Administration. Any conclusions or opinions expressed in this report represent solely those of the author(s) and not necessarily those of The Regents of the University of California, the Lawrence Berkeley Laboratory or the United States Energy Research and Development Administration.

TECHNICAL INFORMATION DIVISION
LAWRENCE BERKELEY LABORATORY
UNIVERSITY OF CALIFORNIA
BERKELEY, CALIFORNIA 94720